LARGE ROTATIONS IN FIRST-ORDER SHEAR DEFORMATION FE ANALYSIS OF LAMINATED SHELLS

Ireneusz Kreja [a,*] and Rüdiger Schmidt [b]

[a] Gdańsk University of Technology, Faculty of Civil and Environmental Engineering, ul.G.Narutowicza 11/12, 80-952 Gdańsk, Poland

[b] RWTH Aachen University, Institute of General Mechanics, Templergraben 64, D-52056 Aachen, Germany

Abstract- The paper deals with the geometrically non-linear analysis of laminated composite beams, plates and shells in the framework of the first-order transverse shear deformation (FOSD) theory. A central point of the present paper is the discussion of the relevance of five- and six-parameter variants, respectively, of the FOSD hypothesis for large rotation plate and shell problems. In particular, it is shown that the assumption of constant through-thickness distribution of the transverse normal displacements is acceptable only for small and moderate rotation problems. Implications inherent in this assumption that are incompatible with large rotations are discussed from the point of view of the transverse normal strain-displacement relations as well as in the light of an enhanced, accurate large rotation formulation based on the use of Euler angles. The latter one is implemented as an updating process within a total Lagrangian formulation of the six-parameter FOSD large rotation plate and shell theory. Numerical solutions are obtained by using isoparametric 8-node Serendipity-type shell finite elements with reduced integration. The Riks-Wempner-Ramm arc-length control method is used to trace primary and secondary equilibrium paths in the pre- and post-buckling range of deformation. A number of sample problems of non-linear, large rotation response of composite laminated plate and shell structures are presented including symmetric and asymmetric snap-through and snap-back problems.

Keywords: composite laminates, multi-layered shells, finite elements, large rotations

1. Introduction

The continuing interest in the accurate modelling of the large deflection behaviour of composite laminated plates and shells has led to the substantiation of a vast number of geometrically non-linear theories that differ (a) with respect to the consideration of transverse shear strains, transverse normal strains, and higher-order effects, (b) with respect to the

---

* Corresponding author, *e-mail address*: ikreja@pg.gda.pl

consideration of finite displacements and rotations, (c) with respect to the number of terms retained in various strain-components, e.g. in variants for thin structures, shallow structures, etc.

Consideration of finite displacements and rotations in plates and shells can be accomplished in different levels, e.g. using (i) the von Kármán-type non-linearity that accounts only for the products and squares of the derivatives of the transverse deflection in the strain-displacement relations; (ii) the non-linearity due to moderate rotations; (iii) the non-linearity due to unrestricted, large rotations.

General shell theories, i.e. theories taking into account higher-order effects by assuming a through-thickness distribution of the displacement field in the form of an arbitrary higher-order series expansion, have been given by Librescu [1], [2] for unrestricted rotations, and by Librescu and Schmidt [3] in the framework of moderate rotation shell theory. Third-order transverse shear deformation (TOSD) theories based on a cubic representation of the displacement field across the shell thickness have been proposed by Reddy [4] for von Kármán-type non-linear plate theory and by Başar, Ding and Schultz [5] for large rotation shell theory. First-order transverse shear deformation (FOSD) theories, i.e. theories assuming a linear variation of the displacement field through the shell thickness have been derived for unrestricted, large rotations by Habip [6], [7] and Habip and Ebcioglu [8], for moderate rotations by Schmidt and Reddy [9], and for thin shells in the framework of von Kármán-type non-linearity by Wempner [10] and Galimov [11], [12]. Geometrically non-linear equivalent single layer theories assuming the FOSD or TOSD hypothesis for each individual layer of a composite shell and reducing the number of kinematical variables by invoking interlayer shear stress continuity conditions and zero shear traction boundary conditions on the upper and lower bounding surfaces have been proposed by Librescu and Schmidt [13], Schmidt and Librescu [14] (layerwise FOSD (zig-zag) theory), and Başar, Ding and Schultz [5] (layerwise TOSD theory), among others.

One of the earliest successful FEM computations for large deformations of laminated shells was described in 1970 by Schmit and Monforton [15], who analysed sandwich plates and cylindrical panels using the Kirchhoff-Love model for the outer faces combined with the honeycomb sandwich core. The concept of degenerated shell elements was applied in [16] within Updated Lagrangian formulation to analyze large deformations of a thin-walled cylinder under internal pressure. Jun and Hong [17] used a very similar model to investigate buckling of laminated cylindrical shells. Degenerated elements within Total Lagrangian formulation were used in [18] and [19]. The Kirchhoff-Love model was applied in [20] for the non-linear FE analysis of imperfect laminated shells. The FE formulation based on the Marguerre shallow shell theory was presented for composite shells in [21]. The FOSD model within the Moderate Rotation Theory was implemented in [22] and extended in [23]. The refined von Kármán TOSD theory for large deformation analysis of composite plates was applied by Reddy [4].

Dennis and Palazotto [24] and Tsai et al. [25] proposed a large rotation formulation for laminated shells based on the TOSD theory; however their approach did not include a proper accumulation of rotations. Similar shortcomings characterize the FE implementations of the FOSD large rotation theory of laminated shells described in [26 - 28].

Up to the authors' knowledge, the first FE application for laminated shells in the range of finite rotations was done by Başar et al. [5], who developed a layer-wise laminated shell theory with the description of finite rotations based on the concept of Euler angles. A similar way of the description of the rotation of the shell director was applied also by Brank et al. in [29], where an effective non-linear formulation is presented for thin multilayered shells assuming a linear distribution of the in-plane strains through the shell thickness and constant transverse shear strains. The updated rotation formulation based on the Rodrigues formula proposed for isotropic shells by Simo et al. [30] has been applied for laminated shells in [31 - 35]. Carrera and Parisch [31] analysed large rotation problems for composite shells

applying a so-called improved FOSD formulation. Başar et al. [32] performed finite rotation analysis using the multi-director FE shell model. Assumed Natural Strain elements with the zig-zag laminated shell model have been used in [33]. Vu-Quoc et al. [34] constructed an elaborate multi-layered model, where the layer directors appear as a chain of rigid links. Balah and Al-Ghamedy [35] presented a FE formulation of a four-node isoparametric shell element based on a TOSD theory.

A quite popular tactic in the treatment of large rotation problems in the analysis of laminated shells consists in the application of three-dimensional shell elements possessing only translational degrees of freedom [36 – 38]. Such an approach allows for using a simple additive scheme for updating the displacement fields but, on the other hand, special techniques should be applied to eliminate locking for thin shells. For this purpose, Kinkel et al. [36] employed Assumed Natural Strain and Enhanced Assumed Strain displacement-based shell elements. Kulikov and Plotnikova [37] applied shell elements based on the Hu-Washizu mixed variational principle whereas Sze and Zheng [38] chose the hybrid-stress formulation. A review of the FE implementations of large rotation analysis must not overlook also the co-rotational formulations developed in [39 - 43]. The proposal of Pai and Palazotto [43] is worthy of a particular notice. As they declared, their Total Lagrangian corotational formulation should be capable to model large rotations and strains including even such second order effect as a variation of the composite stiffness due to the change of fibre direction during the deformation of a laminate.[†] As far as we know, their model has not been confronted with any popular benchmark problem for large deformation of laminated shells. However, the results of a corresponding geometrically-exact curved beam model [45] were very promising and the team decided to tackle with the extremely challenging task of a computer simulation of inflation of a tire [46] though the material properties were assumed as

---

[†] The effect of fibre rotation during deformation was investigated also by Wisnom [44].

linear elastic. A much more advanced large strain model for laminated shells has been proposed by Başar and co-workers [32, 47].

The present paper deals with the geometrically non-linear analysis of beams, plates and shells in the framework of the FOSD theory. The considerations are limited to static problems of laminated shells assuming linear elastic material properties and small strains. Inertia forces, displacement follower loads, deformation dependent stiffness, change of thickness, damage problems of delamination or matrix cracking, as well as, thermal effects and geometrical imperfections are not included in the present formulation. In this context, the main focus of this paper is on the large rotation finite element analysis of laminated composite plate and shell structures with an arbitrary lamination scheme. In linear plate and shell theory the FOSD hypothesis is expressed in terms of five kinematical variables: two tangential mid-surface displacement components and two rotations of the mid-surface constitute a linear through-thickness distribution of the tangential displacement field, whereas the transverse normal displacement of the mid-surface is considered constant across the thickness in order to accommodate the inextensibility of the director. A six-parameter theory with a linear through-thickness distribution of the transverse normal displacement has to be considered only if the thickness change is to be taken into account. In the context of this paper the implications of these five- and six-parameter variants, respectively, of the FOSD hypothesis for non-linear plate and shell problems are discussed. An enhanced, accurate formulation of large rotations in plates and shells based on the use of Euler angles is derived. Based on this formulation it can be shown that the assumption of constant through-thickness distribution of the transverse normal displacements is acceptable only for small and moderate rotation problems, while large rotation problems require a six-parameter approach admitting at least a linear through-thickness distribution of the transverse normal displacement even for inextensibility of the director. The accurate large rotation formulation is implemented as an updating process

within a total Lagrangian formulation of the six-parameter FOSD large rotation plate and shell theory based on the strain-displacement relations of Habip [6], [7] and Habip and Ebcioglu [8]. Numerical solutions are obtained by using isoparametric 8-node Serendipity-type shell finite elements with reduced integration. The Riks-Wempner-Ramm arc-length control method is used to trace primary and secondary equilibrium paths in the pre- and post-buckling range of deformation.

In Section 2 of this paper the incremental Total Lagrangian formulation of the FOSD large rotation theory of composite shells and its finite element discretization is presented. First, in Section 2.1 some basic relations of 3-D kinematics and FOSD large rotation plate and shell theory are summarized. In Section 2.2 the five- and six-parameter variants of the FOSD hypothesis are discussed and an accurate formulation of large rotations in plates and shells is derived. In Section 2.3 the Total Lagrangian formulation of the theory is presented. Section 2.4 gives a brief account of the constitutive equations. In Section 2.5 the finite element method discretization of the problem is given. Finally, Section 2.6 deals with the incremental equilibrium equations of the system and the solution and control methods applied. Section 3 of this paper is devoted to numerical results. Numerical solutions are obtained by using isoparametric 8-node Serendipity-type shell finite elements with reduced integration. The Riks-Wempner-Ramm arc-length control method is used to trace primary and secondary equilibrium paths in the pre- and post-buckling range of deformation. A number of sample problems of non-linear, large rotation response of composite laminated plate and shell structures are presented including symmetric and asymmetric snap-through and snap-back problems. Various simplified non-linear beam, plate and shell theories are used for comparative analysis, like e.g. the FOSD refined von Kármán-type and moderate rotation theory in their respective range of applicability, as well as variants of the large rotation theory

proposed in literature using approximate strain-displacement relations or an approximate approach to large rotations only.

2. Incremental Total Lagrangian Formulation of the First-Order Shear Deformation Large Rotation Theory FEM Analysis of Composite Shells

2.1. Basic assumptions and nomenclature

The motion of the 3-D shell-like body in space is considered assuming the existence of static effects only. According to the Total Lagrangian (TL) incremental formulation, we consider the following three configurations of the body (Fig. 1):

- the initial configuration ^{0}C, at time *0*;

- the actual configuration ^{1}C, at time *t*;
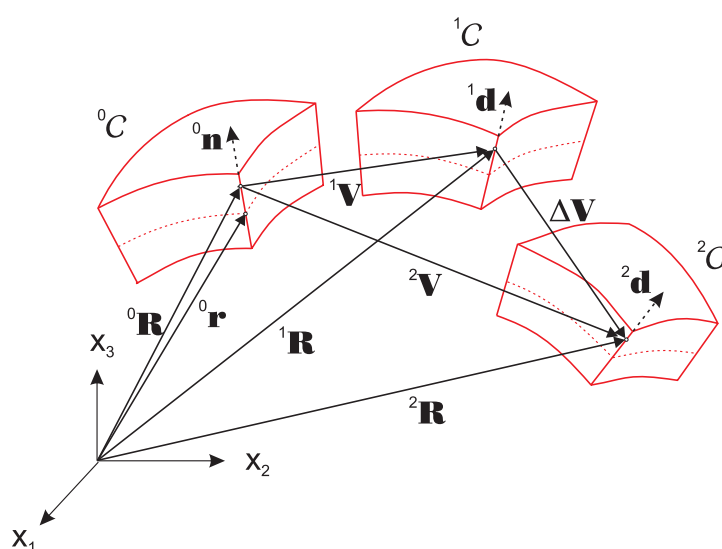
- the searched configuration ^{2}C, at time *t+Δt*.

Fig. 1. Shell body motion in space

The respective configurations are characterized by left superscripts 0, 1, and 2. Thus, the position vector of an arbitrary point P of the configuration ^{m}C is denoted by $^{m}\mathbf{R}$; whereas the time instants ^{0}t, ^{1}t and ^{2}t are used for the time variable equal *0*, *t* and *t+Δt*, respectively.

The position vector $^{m}\mathbf{R}$ can be represented as a function of general convected coordinates θ^{i} (i = 1, 2, 3) and the time variable:

$$^{m}\mathbf{R} = \mathbf{R}(\theta^{1},\theta^{2},\theta^{3},{}^{m}t) \tag{1}$$

The coordinate system (θ^{1}, θ^{2}, θ^{3}) is defined in such a way that θ^{α} (α = 1, 2) denote convected curvilinear surface coordinates of the shell mid-surface Ω, and θ^{3} is the thickness coordinate taking values from the interval (*-h/2*, *h/2*) with *h* standing for the initial shell thickness. In the undeformed configuration the coordinate θ^{3} is measured in the direction that is perpendicular to Ω.

According to the first-order shear deformation (FOSD) Reissner-Mindlin theory it is assumed that straight lines normal to the undeformed shell midsurface remain straight after deformation, but not necessarily normal to the undeformed midsurface. Introducing position vectors of points on the mid-surface $^{m}\Omega$ (in the configuration ^{m}C),

$$^{m}\mathbf{r} = \mathbf{r}(\theta^{\alpha},{}^{m}t) \tag{2}$$

one can write the FOSD hypothesis in the form

$$^{m}\mathbf{R} = {}^{m}\mathbf{r} + \theta^{3\,m}\mathbf{d} . \tag{3}$$

Here $\theta^{3\,m}\mathbf{d}$ is the local position vector of a point in the shell space in the configuration ^{m}C often called "*director*".

With Eq. (3), the displacement vector $^{m}\mathbf{V}$ in configuration ^{m}C is

$$ {}^{m}\mathbf{V} = {}^{m}\mathbf{R} - {}^{0}\mathbf{R} = ({}^{m}\mathbf{r} - {}^{0}\mathbf{r}) + \theta^{3}\,({}^{m}\mathbf{d} - {}^{0}\mathbf{n}) = \overset{m\,(0)}{\mathbf{V}} + \theta^{3}\,\overset{m\,(1)}{\mathbf{V}}. \tag{4} $$

The displacement vector ${}^{m}\mathbf{V}$ can be expressed in terms of components referred to the contravariant base vectors ${}^{0}\mathbf{g}^{i}$, or to the covariant base vectors ${}^{0}\mathbf{g}_{i}$ of the undeformed shell space as

$$ {}^{m}\mathbf{V} = {}^{m}V_{i}\,{}^{0}\mathbf{g}^{i} = {}^{m}V^{i}\,{}^{0}\mathbf{g}_{i}, \tag{5a} $$

and similarly in terms of the components referred to the co- and contravariant base vector triads $({}^{0}\mathbf{a}^{1}, {}^{0}\mathbf{a}^{2}, {}^{0}\mathbf{n})$ and $({}^{0}\mathbf{a_{1}}, {}^{0}\mathbf{a_{2}}, {}^{0}\mathbf{n})$, respectively, of the undeformed shell mid-surface as

$$ {}^{m}\mathbf{V} = {}^{m}\upsilon_{\alpha}\,{}^{0}\mathbf{a}^{\alpha} + {}^{m}\upsilon_{3}\,{}^{0}\mathbf{n} = {}^{m}\upsilon^{\alpha}\,{}^{0}\mathbf{a}_{\alpha} + {}^{m}\upsilon_{3}\,{}^{0}\mathbf{n} \tag{5b} $$

From Eqs. (4) and (5) the FOSD hypothesis follows in the form

$$ {}^{m}\upsilon_{i}(\theta^{1},\theta^{2},\theta^{3}) = \overset{m\,(0)}{\upsilon_{i}}(\theta^{1},\theta^{2}) + \theta^{3}\,\overset{m\,(1)}{\upsilon_{i}}(\theta^{1},\theta^{2}). \tag{6} $$

The Green strain tensor in the shell space is given by

$$ {}^{m}\varepsilon_{ij} = \tfrac{1}{2}\left({}^{m}V_{i}\big\|_{j} + {}^{m}V_{j}\big\|_{i} + {}^{m}V^{k}\big\|_{i}\,{}^{m}V_{k}\big\|_{j} \right) \tag{7} $$

where $(.)\big\|_{i}$ is the covariant derivative with respect to the metric of the undeformed shell space, while ${}^{m}V^{i}$ and ${}^{m}V_{i}$ denote the contra- and covariant components of the displacement vector ${}^{m}\mathbf{V}$ referred to the base vector triads ${}^{0}\mathbf{g}_{i}$ and ${}^{0}\mathbf{g}^{i}$, respectively. They can be related to the components ${}^{m}\upsilon^{i}$ and ${}^{m}\upsilon_{i}$ referred to the reference surface base vector triads as

$$ {}^{m}V_{\alpha} = {}^{0}\mu_{\alpha}^{\beta}\,{}^{m}\upsilon_{\beta}, \qquad {}^{m}V^{\alpha} = \left({}^{0}\mu^{-1}\right)_{\beta}^{\alpha}\,{}^{m}\upsilon^{\beta}, \qquad {}^{m}V^{3} = {}^{m}V_{3} = {}^{m}\upsilon^{3} = {}^{m}\upsilon_{3}, \tag{8} $$

where ${}^{0}\mu_{\alpha}^{\beta}$ and $\left({}^{0}\mu^{-1}\right)_{\beta}^{\alpha}$ denote the components of the shifter tensor and its inverse.

Using Eq. (6) in the framework of FOSD theory the Green strain tensor components can be presented in the form of a power series expansion with respect to the thickness coordinate as follows:

- in-plane and bending terms:

$$
{}^{m}\varepsilon_{\alpha\beta}(\theta^1,\theta^2,\theta^3) = {}^{m}\overset{(0)}{\varepsilon}_{\alpha\beta}(\theta^1,\theta^2) + \theta^3\,{}^{m}\overset{(1)}{\varepsilon}_{\alpha\beta}(\theta^1,\theta^2) + \left(\theta^3\right)^2\,{}^{m}\overset{(2)}{\varepsilon}_{\alpha\beta}(\theta^1,\theta^2)\,,
\tag{9a}
$$

- transverse shear terms:

$$
{}^{m}\varepsilon_{\alpha3}(\theta^1,\theta^2,\theta^3) = {}^{m}\overset{(0)}{\varepsilon}_{\alpha3}(\theta^1,\theta^2) + \theta^3\,{}^{m}\overset{(1)}{\varepsilon}_{\alpha3}(\theta^1,\theta^2)\,,
\tag{9b}
$$

- transverse normal terms:

$$
{}^{m}\varepsilon_{33}(\theta^1,\theta^2,\theta^3) = {}^{m}\overset{(0)}{\varepsilon}_{33}(\theta^1,\theta^2)\,.
\tag{9c}
$$

The above strain components are related to the kinematical variables ${}^{m}\overset{(0)}{\upsilon}_{i}(\theta^1,\theta^2)$

and ${}^{m}\overset{(1)}{\upsilon}_{i}(\theta^1,\theta^2)$ by the following strain-displacement relations (see [6] – [7])

$$
{}^{m}\overset{(0)}{\varepsilon}_{\alpha\beta} = \tfrac{1}{2}\left({}^{m}\overset{(0)}{\varphi}_{\alpha\beta} + {}^{m}\overset{(0)}{\varphi}_{\beta\alpha}\right) + \tfrac{1}{2}\,{}^{m}\overset{(0)}{\varphi}_{\alpha3}\,{}^{m}\overset{(0)}{\varphi}_{\beta3} + \tfrac{1}{2}\,{}^{m}\overset{(0)}{\varphi}_{\lambda\alpha}\,{}^{m}\overset{(0)}{\varphi}{}^{\lambda}_{.\beta}\,,
\tag{10a}
$$

$$
\begin{aligned}
{}^{m}\overset{(1)}{\varepsilon}_{\alpha\beta} = {}&\tfrac{1}{2}\left({}^{m}\overset{(1)}{\varphi}_{\alpha\beta} + {}^{m}\overset{(1)}{\varphi}_{\beta\alpha}\right) - \tfrac{1}{2}\left({}^{0}b^{\lambda}_{\alpha}\,{}^{m}\overset{(0)}{\varphi}_{\lambda\beta} + {}^{0}b^{\lambda}_{\beta}\,{}^{m}\overset{(0)}{\varphi}_{\lambda\alpha}\right) + \\
&+ \tfrac{1}{2}\left({}^{m}\overset{(0)}{\varphi}_{\alpha3}\,{}^{m}\overset{(1)}{\varphi}_{\beta3} + {}^{m}\overset{(0)}{\varphi}_{\beta3}\,{}^{m}\overset{(1)}{\varphi}_{\alpha3}\right) + \tfrac{1}{2}\left({}^{m}\overset{(0)}{\varphi}_{\lambda\alpha}\,{}^{m}\overset{(1)}{\varphi}{}^{\lambda}_{.\beta} + {}^{m}\overset{(1)}{\varphi}_{\lambda\alpha}\,{}^{m}\overset{(0)}{\varphi}{}^{\lambda}_{.\beta}\right),
\end{aligned}
\tag{10b}
$$

$$
{}^{m}\overset{(2)}{\varepsilon}_{\alpha\beta} = -\tfrac{1}{2}\left({}^{0}b^{\lambda}_{\alpha}\,{}^{m}\overset{(1)}{\varphi}_{\lambda\beta} + {}^{0}b^{\lambda}_{\beta}\,{}^{m}\overset{(1)}{\varphi}_{\lambda\alpha}\right) + \tfrac{1}{2}\,{}^{m}\overset{(1)}{\varphi}_{\alpha3}\,{}^{m}\overset{(1)}{\varphi}_{\beta3} + \tfrac{1}{2}\,{}^{m}\overset{(1)}{\varphi}_{\lambda\alpha}\,{}^{m}\overset{(1)}{\varphi}{}^{\lambda}_{.\beta}\,,
\tag{10c}
$$

$$2\,\overset{m}{\varepsilon}{}^{(0)}_{\alpha3} = \overset{m}{\varphi}{}^{(0)}_{\alpha3} + \overset{m}{\upsilon}{}^{(0)}_{\alpha} + \overset{m}{\upsilon}{}^{\lambda}\overset{m}{\varphi}{}^{(1)}_{\lambda\alpha} + \tfrac{1}{2}\overset{m}{\upsilon}{}^{(1)}_3\left(\overset{m}{\varphi}{}^{(0)}_{\lambda3} - \overset{m}{\upsilon}{}^{(1)}_{\alpha}\right) + \tfrac{1}{2}\overset{m}{\upsilon}{}^{(1)}_3\left(\overset{m}{\varphi}{}^{(0)}_{\lambda3} + \overset{m}{\upsilon}{}^{(1)}_{\alpha}\right), \tag{10d}$$

$$2\,\overset{m}{\varepsilon}{}^{(1)}_{\alpha3} = \overset{m}{\upsilon}{}^{(1)}_{3,\alpha} + \overset{m}{\upsilon}{}^{\lambda}\overset{m}{\upsilon}{}^{(1)}_{\lambda}\Big|_{\alpha} - \tfrac{1}{2}\overset{m}{\upsilon}{}^{(1)}_{3,\lambda}\overset{m}{\varphi}{}^{\lambda}_{\cdot\alpha} + \overset{m}{\upsilon}{}^{(1)}_3\overset{m}{\upsilon}{}^{(0)}_{3,\alpha} + \tfrac{1}{2}\overset{m}{\upsilon}{}^{(1)}_{3,\lambda}\overset{m}{\varphi}{}^{\lambda}_{\cdot\alpha}. \tag{10e}$$

$$\overset{m}{\varepsilon}_{33} = \overset{m}{\upsilon}{}^{(1)}_3 + \tfrac{1}{2}\overset{m}{\upsilon}{}^{(1)k}\overset{m}{\upsilon}{}^{(1)}_{k}. \tag{10f}$$

In the above relations the following abbreviations have been used:

$$\overset{m}{\varphi}{}^{(n)}_{\alpha\beta} = \overset{m}{\upsilon}{}^{(n)}_{\alpha}\Big|_{\beta} - {}^{0}b_{\alpha\beta}\,\overset{m}{\upsilon}{}^{(n)}_3, \tag{11a}$$

$$\overset{m}{\varphi}{}^{(n)}_{\alpha3} = \overset{m}{\upsilon}{}^{(n)}_{3,\alpha} + {}^{0}b^{\lambda}_{\alpha}\,\overset{m}{\upsilon}{}^{(n)}_{\lambda}, \tag{11b}$$

$${}^{0}b_{\alpha\beta} = {}^{0}\mathbf{a}_{\alpha,\beta}\cdot{}^{0}\mathbf{n}, \qquad {}^{0}b^{\alpha}_{\beta} = {}^{0}a^{\alpha\lambda}\,{}^{0}b_{\lambda\beta}, \tag{11c}$$

$${}^{0}a^{\alpha\beta} = {}^{0}\mathbf{a}^{\alpha}\cdot{}^{0}\mathbf{a}^{\beta}, \qquad {}^{0}\mathbf{a}_{\alpha} = {}^{0}\mathbf{r}_{,\alpha}. \tag{11d}$$

Here $(\ )|_{\beta}$ and $(\ )_{,\beta}$ denote the covariant and partial derivative with respect to the reference surface coordinates while ${}^{0}b_{\alpha\beta}$ and ${}^{0}b^{\alpha}_{\beta}$ are the covariant and mixed components of the curvature tensor of the mid-surface, respectively.

In the strain-displacement relations (10) all non-linear terms have been marked by single or double lines. For the fully non-linear theory accounting for arbitrarily large rotations all terms have to be taken into account. We will call this theory FOSD 6-parameter large rotation theory (LRT6). Terms marked by a double line can be dropped for moderate rotation theory

(MRT), see [9]. All terms marked by a double or single line can be dropped for linear (small deflection) theory.

2.2. Assumption of the inextensibility of the director

The straightforward interpretation of the director inextensibility assumed in the present considerations results in the following equation:

$$^{m}\varepsilon_{33} = 0 . \tag{12}$$

2.2.1. Simple realization of the director inextensibility resulting in pure 5-parameter theories

In literature most frequently in the FOSD hypothesis (6) only 5 parameters are considered by putting

$$^{m}\overset{(1)}{\upsilon}_{3} = 0 \tag{13a}$$

This leads to the FOSD hypothesis in the form

$$
\begin{aligned}
^{m}\upsilon_{\alpha}(\theta^{1},\theta^{2},\theta^{3}) &= {}^{m}\overset{(0)}{\upsilon}_{\alpha}(\theta^{1},\theta^{2}) + \theta^{3} \, {}^{m}\overset{(1)}{\upsilon}_{\alpha}(\theta^{1},\theta^{2}), \qquad \alpha = 1,2 \\
^{m}\upsilon_{3}(\theta^{1},\theta^{2},\theta^{3}) &= {}^{m}\overset{(0)}{\upsilon}_{3}(\theta^{1},\theta^{2})
\end{aligned}
\tag{13b}
$$

One can treat (13a) as a simple (approximate) realization of the constraint (12) seeing that, according to (10f), $^{m}\overset{(1)}{\upsilon}_{3}$ is equal to the linear (dominating) part of the component $^{m}\varepsilon_{33}$. This postulate leads to simplified strain-displacement relations for five-parameter theory that can be easily obtained from Eqs.(10) by invoking (13) (see e.g. [26 - 28]).

On the other hand, it is well known, that the hypothesis (13b) with only five kinematical parameters is not capable of treating finite rotations (see e.g. [47]). Therefore in the following an enhanced approach will be developed. For the purpose of comparison, however, in this

paper we will also present results obtained with the five-parameter variant of the large rotation theory based on (13) which will be called LRT5. One should notice that the parameters ${}^{m}v_1^{(1)}$ and ${}^{m}v_2^{(1)}$ are often interpreted as the rotations φ_1 and φ_2 about the mid-surface base vectors ${}^{0}\mathbf{a}_2$ and ${}^{0}\mathbf{a}_1$, respectively (see Fig. 2). However, we will show in Chapter 2.2.2, that this holds true only for small and moderate rotations (e.g. linear, small deflection analysis or non-linear analysis based on the refined von Kármán theory or moderate rotation theory (MRT)).
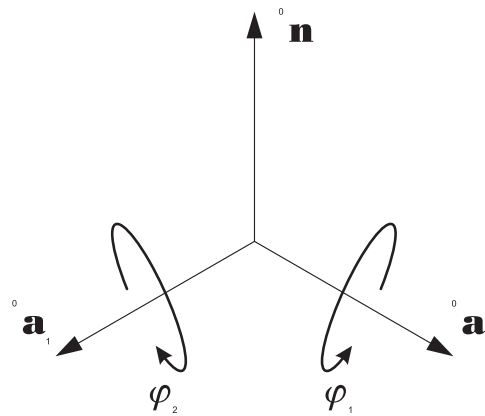
Fig. 2. Rotation angles in FEM models

2.2.2. Enhanced interpretation of rotations

Looking for a more accurate formulation one can express the changes of the inextensible director by using Euler angles (see e.g. [48]). One can assume that the transformation of any vector from the initial configuration ${}^{0}C$ to the configuration ${}^{m}C$ can be achieved by two subsequent rotations, first about the mid-surface base vector ${}^{0}\mathbf{a}_1$, then about ${}^{0}\mathbf{a}_2$. With the two rotation angles from Fig. 2, the matrix operators for such a conversion are as follows:

$$\left[\mathscr{R}_1({}^m\varphi_2)\right] = \begin{bmatrix} 1 & 0 & 0 \\ 0 & \cos({}^m\varphi_2) & \sin({}^m\varphi_2) \\ 0 & -\sin({}^m\varphi_2) & \cos({}^m\varphi_2) \end{bmatrix} \quad \left[\mathscr{R}_2({}^m\varphi_1)\right] = \begin{bmatrix} \cos({}^m\varphi_1) & 0 & \sin({}^m\varphi_1) \\ 0 & 1 & 0 \\ -\sin({}^m\varphi_1) & 0 & \cos({}^m\varphi_1) \end{bmatrix}. \quad (14)$$

and the rotation matrix for the whole transformation can be obtained as

$$\left[\mathscr{R}\right] = \left[\mathscr{R}_2({}^m\varphi_1)\right]\left[\mathscr{R}_1({}^m\varphi_2)\right] = \begin{bmatrix} \cos({}^m\varphi_1) & -\sin({}^m\varphi_1)\sin({}^m\varphi_2) & \sin({}^m\varphi_1)\cos({}^m\varphi_2) \\ 0 & \cos({}^m\varphi_2) & \sin({}^m\varphi_2) \\ -\sin({}^m\varphi_1) & -\cos({}^m\varphi_1)\sin({}^m\varphi_2) & \cos({}^m\varphi_1)\cos({}^m\varphi_2) \end{bmatrix}. \quad (15)$$

In particular, this transformation can be used to describe the director ${}^m\mathbf{d}$ introduced in (3), as the image of the vector ${}^0\mathbf{n}$ obtained by performing subsequent rotations with the rotation angles ${}^m\varphi_2$ and ${}^m\varphi_1$ about the mid-surface base vectors ${}^0\mathbf{a}_1$ and ${}^0\mathbf{a}_2$, respectively:

$$^m\mathbf{d} = \sin({}^m\varphi_1)\cos({}^m\varphi_2)\,{}^0\mathbf{a}^1 + \sin({}^m\varphi_2)\,{}^0\mathbf{a}^2 + \cos({}^m\varphi_1)\cos({}^m\varphi_2)\,{}^0\mathbf{n}. \quad (16)$$

Now, turning back to the relation (4) for the displacement vector ${}^m\mathbf{V}$ in the configuration ${}^m C$, one obtains

$$^m_{(1)}\mathbf{V} = {}^m\mathbf{d} - {}^0\mathbf{n} = \sin({}^m\varphi_1)\cos({}^m\varphi_2)\,{}^0\mathbf{a}^1 + \sin({}^m\varphi_2)\,{}^0\mathbf{a}^2 + \left(\cos({}^m\varphi_1)\cos({}^m\varphi_2) - 1\right){}^0\mathbf{n}. \quad (17)$$

It is obvious that for small and moderate values of the angles ${}^m\varphi_1$ and ${}^m\varphi_2$ one can assume that

$$\sin({}^m\varphi_\alpha) \cong {}^m\varphi_\alpha \qquad \text{and} \qquad \cos({}^m\varphi_\alpha) \cong 1. \quad (18)$$

Thus for small and moderate rotations Eq. (17) yields

$$^m_{(1)}\mathbf{V} \cong {}^m\varphi_1\,{}^0\mathbf{a}^1 + {}^m\varphi_2\,{}^0\mathbf{a}^2 + 0\,{}^0\mathbf{n}. \quad (19)$$

Hence for the small or moderate rotation theory the kinematical hypothesis (13b) is justified, however, as it was already pointed out, this approximation cannot be accepted for large rotations. Therefore the exact relation (17) will be applied in the following derivations for the numerical implementation of the large rotation theory based on the enhanced interpretation of rotations.

For the purpose of the incremental description it is necessary to construct a corresponding relation for the displacement increment. Starting with the Taylor series expansion of the displacement vector at the configuration ^{2}C in the vicinity of the actual configuration ^{1}C, one obtains

$$
\overset{2\,(1)}{\mathbf{V}} = \overset{1\,(1)}{\mathbf{V}} + \overset{(1)}{\Delta\mathbf{V}} \cong \overset{1\,(1)}{\mathbf{V}} + \left.\frac{\partial \overset{(1)}{\mathbf{V}}}{\partial\varphi_1}\right|_t \Delta\varphi_1 + \left.\frac{\partial \overset{(1)}{\mathbf{V}}}{\partial\varphi_2}\right|_t \Delta\varphi_2 \tag{20}
$$

where the higher-order terms were neglected. As a consequence the linearized incremental relation reads

$$
\begin{bmatrix} \overset{(1)}{\Delta\upsilon_1} \\ \overset{(1)}{\Delta\upsilon_2} \\ \overset{(1)}{\Delta\upsilon_3} \end{bmatrix} = \begin{bmatrix} \cos(^{1}\varphi_1)\cos(^{1}\varphi_2) & -\sin(^{1}\varphi_1)\sin(^{1}\varphi_2) \\ 0 & \cos(^{1}\varphi_2) \\ -\sin(^{1}\varphi_1)\cos(^{1}\varphi_2) & -\cos(^{1}\varphi_1)\sin(^{1}\varphi_2) \end{bmatrix} \begin{bmatrix} \Delta\varphi_1 \\ \Delta\varphi_2 \end{bmatrix} \tag{21}
$$

Also, it is quite obvious that the exact relation that can be obtained taking advantage of formula (17) reads:

$$
\overset{(1)}{\Delta\mathbf{V}} = \overset{2\,(1)}{\mathbf{V}} - \overset{1\,(1)}{\mathbf{V}} = \left(\sin(^{2}\varphi_1)\cos(^{2}\varphi_2) - \sin(^{1}\varphi_1)\cos(^{1}\varphi_2)\right){}^{0}\mathbf{a}^1 + \\ + \left(\sin(^{2}\varphi_2) - \sin(^{1}\varphi_2)\right){}^{0}\mathbf{a}^2 + \left(\cos(^{2}\varphi_1)\cos(^{2}\varphi_2) - \cos(^{1}\varphi_1)\cos(^{1}\varphi_2)\right){}^{0}\mathbf{n} \tag{22}
$$

Assuming now the usual incremental decomposition $^{2}\varphi_\alpha = {}^{1}\varphi_\alpha + \Delta\varphi_\alpha$ and additionally taking

$$
\sin(\Delta\varphi_\alpha) \cong \Delta\varphi_\alpha \qquad \text{and} \qquad \cos(\Delta\varphi_\alpha) \cong 1 \tag{23}
$$

one gets from (22) exactly the same relation as (21).

Consequently we obtain a numerical formulation based on the increments of 5 parameters similar as in the LRT5 formulation. Nevertheless, it should be stressed that the approximated relation (21) is used only during the increment and the order of such an approximation is within the range of the usual linearization approximation applied in the incremental Lagrangian formulation. It is important that after the increment is performed the new configuration must be updated according to the exact relation

$$
\begin{bmatrix} {}^{2}\overset{(1)}{\upsilon}_{1} \\ {}^{2}\overset{(1)}{\upsilon}_{2} \\ {}^{2}\overset{(1)}{\upsilon}_{3} \end{bmatrix} = \begin{bmatrix} \cos(\Delta\varphi_1) & -\sin(\Delta\varphi_1)\sin(\Delta\varphi_2) & \sin(\Delta\varphi_1)\cos(\Delta\varphi_2) \\ 0 & \cos(\Delta\varphi_2) & \sin(\Delta\varphi_2) \\ -\sin(\Delta\varphi_1) & -\cos(\Delta\varphi_1)\sin(\Delta\varphi_2) & \cos(\Delta\varphi_1)\cos(\Delta\varphi_2) \end{bmatrix} \begin{bmatrix} {}^{1}\overset{(1)}{\upsilon}_{1} \\ {}^{1}\overset{(1)}{\upsilon}_{2} \\ {}^{1}\overset{(1)}{\upsilon}_{3}+1 \end{bmatrix} - \begin{bmatrix} 0 \\ 0 \\ 1 \end{bmatrix}. \qquad (24)
$$

It is necessary to note that the transformation based on the Euler angles yields a unique result only for angles from the interval ($-\pi/2$; $\pi/2$) (see e.g. [48]), however in the present formulation this restriction applies only to the increments of the rotations and not to the total rotations (see also [49]).

It is essential to understand also that the updating process as described by (24) is applied in every equilibrium iteration before the balanced forces are established. Such a strategy accompanied by a suitable incremental-iterative procedure with a flexible size of load increment guaranties the desired accuracy of the analysis.

One should remember that the 6 parameters which are necessary to describe the displacement vector ${}^{m}\mathbf{V}$ as given in Eq.(4) (${}^{m}\overset{(0)}{\upsilon}_{i}$ and ${}^{m}\overset{(1)}{\upsilon}_{i}$, i =1, 2, 3) must be continuously stored and updated during the analysis. It is quite obvious that such a formulation is not a real "six-

parameter theory", neither a "five-parameter theory", therefore in the present paper it will be referred to as the "LRT56" formulation‡.

2.3. Total Lagrangian formulation

The virtual work principle states equilibrium between the internal virtual work, $^{2}\delta W_{\mathrm{i}}$, and the external virtual work, $^{2}\delta W_{\mathrm{e}}$, in configuration ^{2}C. Within the Total Lagrangian formulation [51] the internal virtual work in ^{2}C that is yet to be determined can be represented as the integral in the known, initial configuration ^{0}C

$$^{2}\delta\mathrm{W}_{\mathrm{i}} = \int\limits_{^{0}\Omega}\left(\sum_{n=0}^{2}{_{0}^{2}}\overset{(n)}{L}{}^{\alpha\beta}\ \delta\,{_{0}^{2}}\overset{(n)}{\varepsilon}_{\alpha\beta} + 2\sum_{n=0}^{1}{_{0}^{2}}\overset{(n)}{L}{}^{\alpha 3}\ \delta\,{_{0}^{2}}\overset{(n)}{\varepsilon}_{\alpha 3}\right){}^{0}d\Omega, \tag{25}$$

where the n-th order stress resultants obtained in the pre-integration through the shell thickness are

$$_{0}^{2}\overset{(n)}{L}{}^{ij} = \int\limits_{-\frac{h}{2}}^{\frac{h}{2}}{_{0}^{2}}S^{ij}\left(\theta^{3}\right)^{n}\ {}^{0}\mu\,d\theta^{3}\,. \tag{26}$$

Here $_{0}^{2}S^{mn}$ are the components of the second Piola-Kirchhoff stress tensor, $_{0}^{2}\varepsilon_{mn}$ denote the components of the Green-Lagrange strain tensor, and $^{0}\mu$ stands for the determinant of the shifter tensor in the initial configuration ^{0}C.

The incremental decomposition of the stress tensor in the configuration ^{2}C can be expressed for the stress resultants as

---

‡ A similar treatment of large rotations was applied for isotropic shells in [50] and for composite shells in [5] and [29].

$$\overset{(n)}{\underset{0}{2}}L^{ij} = \overset{(n)}{\underset{0}{1}}L^{ij} + \overset{(n)}{\underset{0}{}}L^{ij} .$$ (27)

2.4. Constitutive relations

A typical composite shell made of orthotropic fibre-reinforced material can be analysed as a layered structure, with the fibres of the reinforcement in each lamina placed in the surfaces parallel to the shell mid-surface. It is assumed that the orthogonal system of the material axes (a, b, c) in each lamina is introduced in such a way that the a-axis is aligned with the direction of the reinforcement whereas the c-axis is normal to the shell mid-surface. The transverse isotropic material properties ($E_b = E_c$ and $\nu_{ab} = \nu_{ac}$) together with the inextensibility of the director postulated throughout this report allow writing the 3-D incremental constitutive relation for an individual lamina in the material axes:

$$\begin{Bmatrix} _0S^{aa} \\ _0S^{bb} \\ _0S^{ab} \\ _0S^{bc} \\ _0S^{ca} \end{Bmatrix} = [\boldsymbol{C}_m] \begin{Bmatrix} _0\varepsilon_{aa} \\ _0\varepsilon_{bb} \\ 2\,_0\varepsilon_{ab} \\ 2\,_0\varepsilon_{bc} \\ 2\,_0\varepsilon_{ca} \end{Bmatrix} .$$ (28)

with the constitutive matrix

$$[\boldsymbol{C}_m] = \begin{bmatrix} \dfrac{E_a}{1-\nu_{ab}\nu_{ba}} & \dfrac{\nu_{ab}E_a}{1-\nu_{ab}\nu_{ba}} & 0 & 0 & 0 \\ \dfrac{\nu_{ab}E_a}{1-\nu_{ab}\nu_{ba}} & \dfrac{E_b}{1-\nu_{ab}\nu_{ba}} & 0 & 0 & 0 \\ 0 & 0 & G_{ab} & 0 & 0 \\ 0 & 0 & 0 & \kappa G_{bc} & 0 \\ 0 & 0 & 0 & 0 & \kappa G_{ca} \end{bmatrix} .$$ (29)

The set of well known engineering constants (E_i, ν_{ij} and G_{ij}) in (29) is supplemented by the shear correction factor κ, which is taken here to be equal to $^5/_6$.

The transformation of stress and strain vectors between the material axes (a, b, c) and coordinate system ($\theta^1, \theta^2, \theta^3$) can be illustrated by the relations

$$
\begin{Bmatrix} {}_0\varepsilon_{aa} \\ {}_0\varepsilon_{bb} \\ 2{}_0\varepsilon_{ab} \\ 2{}_0\varepsilon_{bc} \\ 2{}_0\varepsilon_{ca} \end{Bmatrix} = [\boldsymbol{T}] \cdot \begin{Bmatrix} {}_0\varepsilon_{11} \\ {}_0\varepsilon_{22} \\ 2{}_0\varepsilon_{12} \\ 2{}_0\varepsilon_{23} \\ 2{}_0\varepsilon_{31} \end{Bmatrix} \qquad \text{and} \qquad \begin{Bmatrix} {}_0S^{11} \\ {}_0S^{22} \\ {}_0S^{12} \\ {}_0S^{23} \\ {}_0S^{31} \end{Bmatrix} = [\boldsymbol{T}]^T \cdot \begin{Bmatrix} {}_0S^{aa} \\ {}_0S^{bb} \\ {}_0S^{ab} \\ {}_0S^{bc} \\ {}_0S^{ca} \end{Bmatrix} \tag{30}
$$

with the transformation matrix

$$
[\boldsymbol{T}] = \left[\begin{array}{ccc|cc} \cos^2(\alpha_k) & \sin^2(\alpha_k) & \frac{1}{2}\sin(2\alpha_k) & 0 & 0 \\ \sin^2(\alpha_k) & \cos^2(\alpha_k) & -\frac{1}{2}\sin(2\alpha_k) & 0 & 0 \\ \sin(2\alpha_k) & -\sin(2\alpha_k) & \cos(2\alpha_k) & 0 & 0 \\ \hline 0 & 0 & 0 & \cos(\alpha_k) & \sin(\alpha_k) \\ 0 & 0 & 0 & -\sin(\alpha_k) & \cos(\alpha_k) \end{array} \right] \tag{31}
$$

where the ply orientation angle, α_k, is measured between the a-axis and the θ^1–axis as shown in Fig. 3.
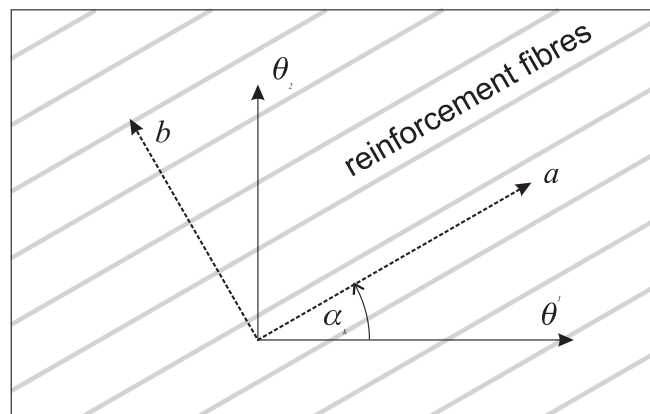
Fig. 3. Ply orientation angle

After the transformation the incremental constitutive relation for an individual lamina in the coordinate system ($\theta^1, \theta^2, \theta^3$) reads:

$$\begin{Bmatrix} {}_0S^{11} \\ {}_0S^{22} \\ {}_0S^{12} \\ {}_0S^{23} \\ {}_0S^{31} \end{Bmatrix} = [C] \begin{Bmatrix} {}_0\varepsilon_{11} \\ {}_0\varepsilon_{22} \\ 2\,{}_0\varepsilon_{12} \\ 2\,{}_0\varepsilon_{23} \\ 2\,{}_0\varepsilon_{31} \end{Bmatrix} \tag{32}$$

where

$$[C] = [T]^T [C_m][T] \tag{33}$$

Performing the pre-integration of the 3-D constitutive relations through the thickness of the whole shell one obtains the 2-D constitutive relation

$$\{{}_0S\} = [H]\{{}_0E\}. \tag{34}$$

The detailed structure of the constitutive relation (34) can be found in [23].

With (34) and (27) the internal work (25) expression can be re-written as

$$ {}^2\delta W_i = \int\limits_{{}^0\Omega} \left(\delta_0^2\varepsilon_{\alpha\beta}\, {}_0^1L^{\alpha\beta} + 2\,\delta_0^2\varepsilon_{\alpha3}\, {}_0^1L^{\alpha3} + \delta_0^2\varepsilon_{\alpha\beta}\, H^{\alpha\beta\chi\delta}\, {}_0\varepsilon_{\chi\delta} + 4\delta_0^2\varepsilon_{\alpha3}\, \Xi^{\alpha\beta}\, {}_0\varepsilon_{\beta3} \right) {}^0d\Omega \tag{35}$$

where $H^{\alpha\beta\chi\delta}$ and $\Xi^{\alpha\beta}$ represent appropriate components of the constitutive matrix $[H]$.

2.5. Finite element method discretization of the problem

Using the isoparametric formulation, the geometry described by the position vector can be interpolated inside each finite element as follows:

$$ {}^m\mathbf{R}(r,s) = \sum_{k=1}^{NNE} \left(N_k(r,s)\, {}^m\mathbf{r}^k \right) + \theta^3 \sum_{k=1}^{NNE} \left(N_k(r,s)\, {}^m\mathbf{d}^k \right), \tag{36}$$

where ${}^{m}\mathbf{r}^{k}$ is the position vector of the node k, with r and s standing for the element natural coordinates, N_k represents the shape function associated with node k, and, finally, NNE means the number of nodes of the element.

The displacement field can be interpolated in an analogous way as the geometry:

$$ {}^{m}\mathbf{V}(r,s) = \sum_{k=1}^{NNE}\left(N_k(r,s)\ {}^{m}\overset{(0)}{\mathbf{V}}{}^{k} \right) + \theta^3 \sum_{k=1}^{NNE}\left(N_k(r,s)\ {}^{m}\overset{(1)}{\mathbf{V}}{}^{k} \right). \tag{37} $$

For the sake of the simplified notation in the following derivations a specific substitution has been introduced

$$ \begin{aligned} {}^{m}u_M &= {}^{m}\overset{(0)}{\upsilon}{}_{i} \quad for \quad M = i = 1,2,3 \\ {}^{m}u_N &= {}^{m}\overset{(1)}{\upsilon}{}_{j} \quad for \quad N-3 = j = 1,2,3 \end{aligned}. \tag{38} $$

With (38) one can construct a quite general form of the strain-displacement relations given in (9) and (10)

$$ {}^{m}_{0}\varepsilon_{ij} = B_{ijM}\ {}^{m}u_M + \tfrac{1}{2}G_{ikP}\,G_{jkQ}\ {}^{m}u_P\ {}^{m}u_Q \ , \tag{39} $$

where B_{ijM} and G_{kjP} stand for two linear operators. Note that here an index notation has been applied because the matrix notation, which was used in our previous paper [23], will not be useful for some of the following transformations.

With (17) and (37) the displacement components u_I can be expressed by the nodal displacement parameters as

$$
{}^{m}u_{M}(r,s) = \sum_{k=1}^{NNE}\left\{ N_{k}(r,s)\,{}^{m}q_{M}^{k}\right\}\quad for \quad M=1,2,3
$$

$$
{}^{m}u_{4}(r,s) = \sum_{k=1}^{NNE}\left\{ N_{k}(r,s)\sin({}^{m}q_{4}^{k})\cos({}^{m}q_{5}^{k})\right\}
$$

$$
{}^{m}u_{5}(r,s) = \sum_{k=1}^{NNE}\left\{ N_{k}(r,s)\sin({}^{m}q_{5}^{k})\right\}
$$

$$
{}^{m}u_{6}(r,s) = \sum_{k=1}^{NNE}\left\{ N_{k}(r,s)\cos({}^{m}q_{4}^{k})\cos({}^{m}q_{5}^{k})\right\}-1
$$

, (40)

where ${}^{m}q_{I}^{k}$ represent the corresponding displacement parameters at the node k. One should note that due to the use of the exact formula (17) the six displacement parameters are expressed in (40) as a non-linear function of five nodal parameters, while the use of the simplified variant (19) would lead to linear relations only.

The derivatives of the strain tensor components with respect to the nodal displacement parameters at the actual configuration, ${}^{1}C$, will be calculated next as

$$
\frac{\partial \varepsilon_{ij}}{\partial q_{R}} = B_{ijM}\,\frac{\partial u_{M}}{\partial q_{R}} + G_{ikP}\,G_{jkM}\,{}^{1}u_{P}\,\frac{\partial u_{M}}{\partial q_{R}}, \tag{41}
$$

$$
\frac{\partial^{2}\varepsilon_{ij}}{\partial q_{R}\,\partial q_{Q}} = \left(B_{ijM} + G_{ikP}\,G_{jkM}\,{}^{1}u_{P}\right)\frac{\partial^{2}u_{M}}{\partial q_{R}\,\partial q_{Q}} + G_{ikP}\,G_{jkM}\,\frac{\partial u_{P}}{\partial q_{Q}}\,\frac{\partial u_{M}}{\partial q_{R}}. \tag{42}
$$

At this stage one should notice that due to the non-linear (trigonometric) relation introduced in (40), the second derivative of the displacement with respect to the nodal displacement parameter does not vanish, in contrast to the simplified formulation LRT5 where the second derivative of the linear relation (19) is zero.

The derivatives given above are used in the linearized expression for the variation of the strain tensor components

$$
\delta({}_{0}^{2}\varepsilon_{ij}) \cong \frac{\partial \varepsilon_{ij}}{\partial q_{S}}\,\delta q_{S} + \frac{\partial^{2}(\varepsilon_{ij})}{\partial q_{S}\,\partial q_{T}}\,\delta q_{S}\,\Delta q_{T}, \tag{43}
$$

and for the strain increment

$$\Delta\varepsilon_{ij} \cong \frac{\partial\varepsilon_{ij}}{\partial q_S}\Delta q_S \,, \tag{44}$$

Now the expression for the internal virtual work can be presented as

$$
{}^2\delta W_i = \delta q_S\underbrace{\left[\int\limits_{{}^0\Omega}\left(\frac{\partial\varepsilon_{\alpha\beta}}{\partial q_S}\,{}_0^1L^{\alpha\beta} + 2\frac{\partial\varepsilon_{\alpha3}}{\partial q_S}\,{}_0^1L^{\alpha3}\right){}^0d\Omega\right]}_{{}_0^1F_S} +
$$
$$
+ \delta q_S\underbrace{\left[\int\limits_{{}^0\Omega}\left(\frac{\partial\varepsilon_{\alpha\beta}}{\partial q_S}\,\mathrm{H}^{\alpha\beta\chi\delta}\,\frac{\partial\varepsilon_{\chi\delta}}{\partial q_T} + 4\frac{\partial\varepsilon_{\alpha3}}{\partial q_S}\,\Xi^{\alpha\beta}\,\frac{\partial\varepsilon_{\beta3}}{\partial q_T}\right){}^0d\Omega\right]}_{{}_0^1K^{(U)}{}_{ST}}\Delta q_T +
$$
$$
+ \delta q_S\underbrace{\left[\int\limits_{{}^0\Omega}\left(\frac{\partial^2(\varepsilon_{\alpha\beta})}{\partial q_S\,\partial q_T}\,{}_0^1L^{\alpha\beta} + 2\frac{\partial^2(\varepsilon_{\alpha3})}{\partial q_S\,\partial q_T}\,{}_0^1L^{\alpha3}\right){}^0d\Omega\right]}_{{}_0^1K^{(G)}{}_{ST}}\Delta q_T +
$$
$$
+ \delta q_S\underbrace{\left[\int\limits_{{}^0\Omega}\left(\frac{\partial^2(\varepsilon_{\alpha\beta})}{\partial q_S\,\partial q_T}\,\mathrm{H}^{\alpha\beta\chi\delta}\,\frac{\partial\varepsilon_{\chi\delta}}{\partial q_R} + 4\frac{\partial^2(\varepsilon_{\alpha3})}{\partial q_S\,\partial q_T}\,\Xi^{\alpha\beta}\,\frac{\partial\varepsilon_{\beta3}}{\partial q_R}\right){}^0d\Omega\right]}_{{}_0^1K^{(II)}{}_{STR}}\Delta q_T\Delta q_R \tag{45}
$$

or in the compact form

$$
{}^2\delta W_i = \delta q_S\left[{}_0^1F_S + \left({}_0^1K^{(U)}{}_{ST} + {}_0^1K^{(G)}{}_{ST}\right)\Delta q_T + \underbrace{{}_0^1K^{(II)}{}_{STR}\Delta q_T\,\Delta q_R}_{J_S}\right] \tag{46}
$$

where the notation marked in (45) has been used.

According to the commonly accepted FEM terminology the particular entities of (46) can be named as follows

- ${}_0^1F_S$ stands for the components of the balanced forces vector in the configuration ${}^1C$, $\left\{{}_0^1\mathbf{F}\right\}$;

- $_{0}^{1}K^{(U)}{}_{ST}$ represents the first part of the incremental stiffness matrix containing the constitutive stiffness term and the initial displacement stiffness term, $\left[_{0}^{1}\mathbf{K}_{u}\right]$;

- $_{0}^{1}K^{(G)}{}_{ST}$ denotes the components of the geometrical stiffness matrix, $\left[_{0}^{1}\mathbf{K}_{g}\right]$;

- $_{0}^{1}K^{(II)}{}_{STR}$ symbolizes the additional object, which according to Kleiber [52] one can call "the second-order stiffness matrix"; the product $\left(_{0}^{1}K^{(II)}{}_{STR}\Delta q_{T}\,\Delta q_{R}\right)$ can be understood as component of the vector $\left\{\mathbf{J}(^{1}\mathbf{q},\Delta\mathbf{q})\right\}$, containing additional terms, which are non-linear with respect to the displacement increments $\left\{\Delta\mathbf{q}\right\}$.

The matrix form of (46) reads

$$^{2}\delta\mathrm{W}_{i} = \left\{\delta\mathbf{q}\right\}^{T}\left(\left\{_{0}^{1}\mathbf{F}\right\}+\left(\left[_{0}^{1}\mathbf{K}_{u}\right]+\left[_{0}^{1}\mathbf{K}_{g}\right]\right)\left\{\Delta\mathbf{q}\right\}+\left\{\mathbf{J}(^{1}\mathbf{q},\Delta\mathbf{q})\right\}\right) \quad . \tag{47}$$

Adopting the external virtual work in its most general form as

$$^{2}\delta\mathrm{W}_{e} = \left\{\delta\mathbf{q}\right\}^{T}\left\{_{0}^{2}\mathbf{R}\right\}, \tag{48}$$

with $\left\{_{0}^{2}\mathbf{R}\right\}$ standing for the vector of nodal forces due to the loads acting in the configuration ^{2}C, one can obtain together with (47) the incremental equilibrium equations as

$$\left(\left[_{0}^{1}\mathbf{K}_{u}\right]+\left[_{0}^{1}\mathbf{K}_{g}\right]\right)\left\{\Delta\mathbf{q}\right\} = \left\{_{0}^{2}\mathbf{R}\right\}-\left\{_{0}^{1}\mathbf{F}\right\}-\left\{\mathbf{J}(^{1}\mathbf{q},\Delta\mathbf{q})\right\}. \tag{49}$$

This is a standard form of the incremental equation of the quasi-static motion of the structure and most of the terms have been efficiently explained by the extended formula (45). However, the geometrical stiffness matrix needs an additional comment. With (42) the expression for the components $_{0}^{1}K^{(G)}{}_{ST}$ can be written in a more detailed form as

$$
{}_0^1 K^{(G)}{}_{ST} = \underbrace{\int_{{}^0\Omega} \left(G_{\alpha kP}\, G_{\beta kM}\, \frac{\partial u_P}{\partial q_S}\, \frac{\partial u_M}{\partial q_T}\, {}_0 L^{\alpha\beta} + 2\, G_{\alpha kP}\, G_{3kM}\, \frac{\partial u_P}{\partial q_S}\, \frac{\partial u_M}{\partial q_T}\, {}_0 L^{\alpha 3} \right) {}^0 d\Omega}_{{}_0^1 K^{(G1)}{}_{ST}} +
$$

$$
+ \underbrace{\int_{{}^0\Omega} \left(\left(B_{\alpha\beta M} + G_{\alpha kP}\, G_{\beta kM}\, {}^1 u_P \right) \frac{\partial^2 u_M}{\partial q_S\, \partial q_T}\, {}_0 L^{\alpha\beta} + 2 \left(B_{\alpha 3 M} + G_{\alpha kP}\, G_{3kM}\, {}^1 u_P \right) \frac{\partial^2 u_M}{\partial q_S\, \partial q_T}\, {}_0 L^{\alpha 3} \right) {}^0 d\Omega}_{{}_0^1 K^{(G2)}{}_{ST}}
$$

$$
\tag{50}
$$

where the geometrical stiffness matrix is split into two parts. The first part of the geometrical stiffness matrix, ${}_0^1 K^{(G1)}{}_{ST}$ is a "regular" geometrical stiffness matrix that is present in every standard TL formulation. However, the additional part, denoted as ${}_0^1 K^{(G2)}{}_{ST}$, results from a non zero value of the second displacement derivative taken with respect to the nodal displacement parameters, which appears in the first term of (42). As it was shown earlier, the non-zero value of that derivative is characteristic for the LRT56 formulation utilizing the trigonometric relation (17), while for the LRT5 formulation based on the linearized relation (19) this derivative vanishes and, as a consequence, the ${}_0^1 K^{(G2)}{}_{ST}$ part does not appear in LRT5. Up to the authors' knowledge, the essential role of that additional part of the geometrical stiffness matrix was indicated for the first time for the non-linear analysis of beams by Frey and Cescotto in [53] (see also [54] for axisymmetric shells, [50] for the degenerated shell finite elements and [55] for the generalized formulation for finite elements with rotational degrees of freedoms).

2.6. Incremental equilibrium equations of the system

A standard aggregation of equilibrium equations (49) for all finite elements results in the following incremental equilibrium equation for the whole FE model:

$$
{}^1\mathbf{K}\, \Delta\mathbf{u} = {}^2\mathbf{R} - {}^1\mathbf{F} - \mathbf{J}({}^1\mathbf{u}, \Delta\mathbf{u}) , \tag{51}
$$

where $\Delta\mathbf{u}$ is the global vector of displacement increments, $^{1}\mathbf{K}$ denotes the global incremental stiffness matrix, $^{2}\mathbf{R}$ is the global load vector in configuration ^{2}C, $^{1}\mathbf{F}$ stands for the global vector of balanced forces in the actual configuration ^{1}C.

Due to the existence of the non-linear term $\mathbf{J}(^{1}\mathbf{u}, \Delta\mathbf{u})$ in (51), the iteration process of the standard Newton-Raphson method is employed to solve this equation. Additionally, the Riks-Wempner-Ramm arc-length control method [56] has been implemented in the present algorithm to allow for tracing also complex equilibrium paths.

3. Numerical examples

3.1. Instability of clamped-hinged circular arch subjected to point load

We start with a relatively simple problem of a circular arch made of isotropic material subjected to a point load at the crown. Its big advantage is the availability of the analytical solution given in [57] for the highly non-linear response with no restrictions imposed on the magnitudes of the deflections and rotations. This example allows testing the ability of the proposed algorithm to analyze problems with very large rotations and to examine the influence of different terms in the strain-displacement relations.

The arch geometry is characterized by the subtending angle $\alpha = 215$ degrees as presented in Fig. 4.
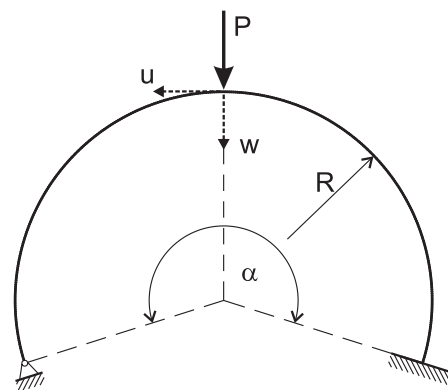
Fig. 4. Clamped-hinged arch, $\alpha = 215$ degrees

In Fig. 5 the graph of the normalized vertical displacement, w/R of the crown point is presented versus the dimensionless load PR^2/EI (with R being the radius of the arch, P the vertical force acting at the crown, E the Young's modulus and I the moment of inertia of the cross-sectional area). The corresponding graph of the normalized horizontal displacement, u/R of the crown point versus the dimensionless load PR^2/EI is given in Fig. 6. The analysed model of the arch consists of twenty 8-URI elements.
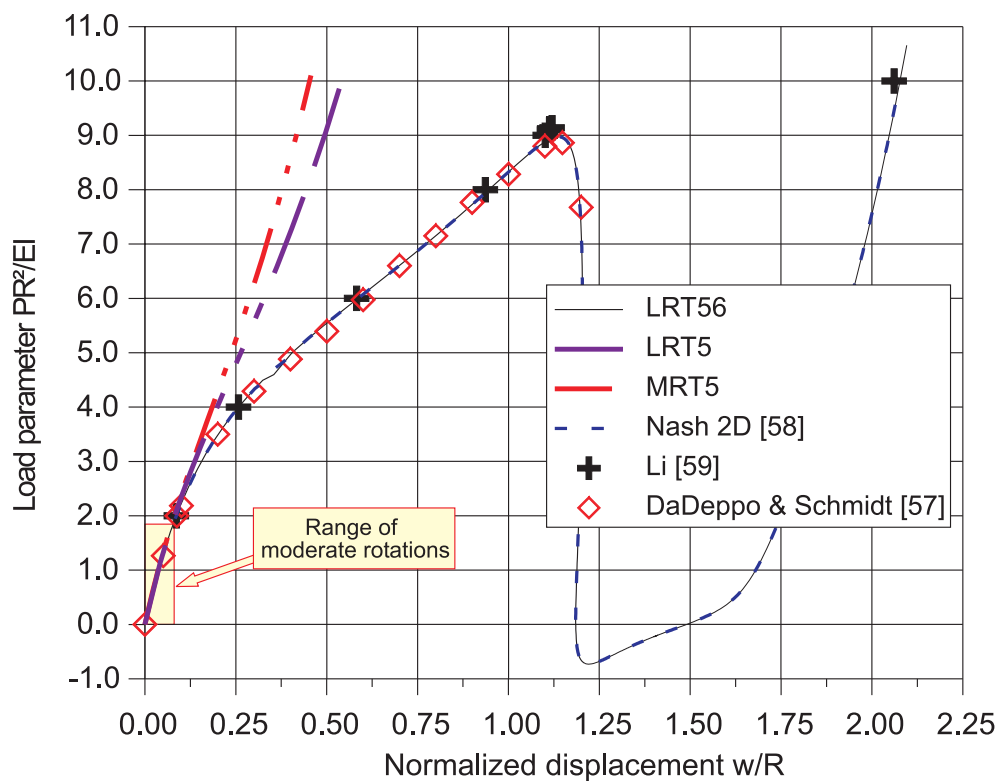
Fig. 5. Normalized downward displacement at the crown for the 215 degrees arch

The results obtained with LRT56 agree very well with the analytical solution as far as it was given in [57]. Since the present analysis goes far beyond the limit point an additional reference solution obtained with a degenerated beam type element [58] has been provided for the sake of comparison and again a very good agreement has been obtained in the entire post-buckling range (see Fig. 5 and Fig. 6). The arch was analysed also in [59] by Li who gave just eight points of the equilibrium path in the pre-buckling range and one separate point after the snap-through took place. Those points correspond quite well with the LRT56 solution (see Fig. 5 and Fig. 6) but in the vicinity of the limit point Li's solution [59] shows differences with LRT56 and with the analytical solution of DaDeppo and Schmidt [57] as well. The

MRT5 model provides excellent results in the range of validity of the theory as marked on Fig. 5. In this example the importance of the proper updating procedure of the rotations is manifested by the big discrepancy of the LRT5 solution where not only quantitative differences can be observed, but even a qualitatively different response of the structure is predicted (see Fig. 5 and Fig. 6). The range of acceptable accuracy of the LRT5 approach is only slightly bigger than that of MRT5.
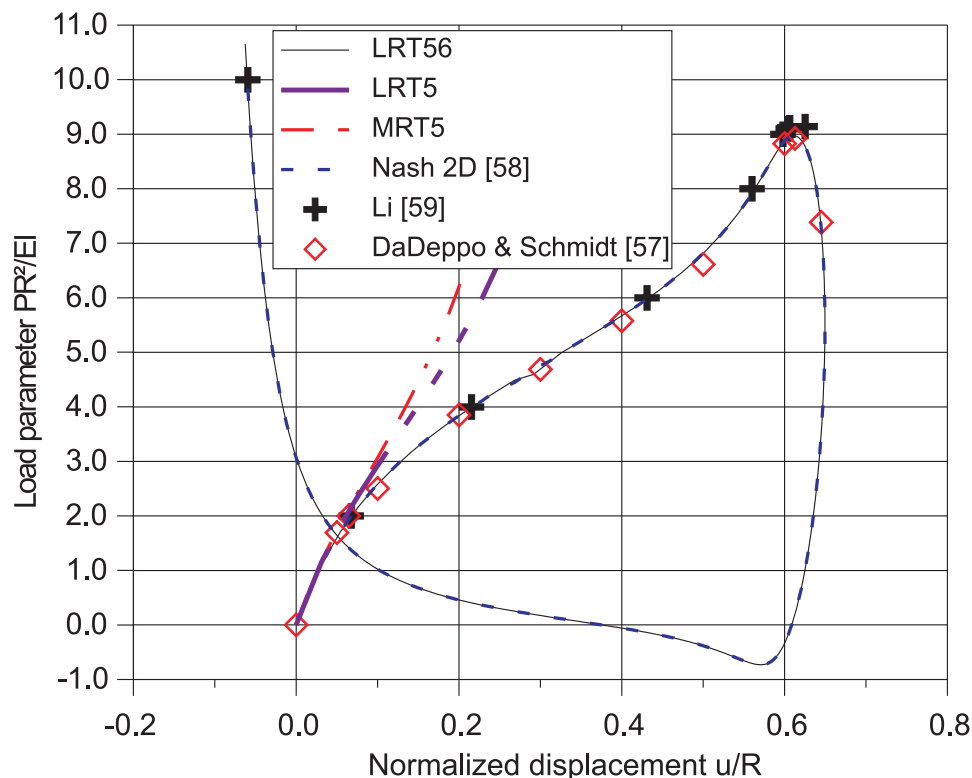
Fig. 6. Normalized horizontal displacement at the crown for the 215 degrees arch

Quite recently Kapania and Li [60] presented their solution of the problem obtained with geometrically exact curved beam elements. As far as it is possible to recognize from the figure given in [60] one can observe an excellent agreement of their solution with the LRT56 results (see Table 1 for a comparison of the limit load points).

It should be mentioned that the main purpose of the presented example was to test the behaviour of the numerical model although the authors are aware that the response of a real

structure can differ from the presented solution due to a possible contact between the deformed beam and the support in the post-buckling region (see [61]).

Table 1.
Comparison of limit load points for the clamped-hinged 215 degrees arch

Model	Max. limit point	Min. limit point
LRT56	8.9712	-0.7304
NASH2D [58] (3-noded isotropic beam element)	8.9718	-0.7306
Kapania and Li [60] (4-noded curved beam element)	8.9727	-0.7360
DaDeppo and Schmidt [57] (analytical)	8.97	-

3.2. Clamped laminated shallow arch under point load

The symmetrical buckling of the shallow circular laminated arch considered next has been analysed earlier in [18] by means of degenerated shell elements. The geometry of the analysed arch is presented in Fig. 7 with R=100 in, h=2 in, $\beta = 0.707$ and the width of the arch is taken as equal to 1 in. Due to the symmetry of the problem half of the arch has been modelled with five 8-URI elements. The material properties used are $E_a = 25 \cdot 10^6$ psi, $E_b = 1 \cdot 10^6$ psi, $G_{ac} = 5 \cdot 10^5$ psi, $G_{ac} = 5 \cdot 10^5$ psi, $G_{bc} = 5 \cdot 10^5$ psi and $\nu_{ab} = 0.25$. The arch consists of two layers, each layer has the same thickness 1 in and is made of the same orthotropic material, but a different ply orientation has been used in each layer. The ply lay-up for the considered example is (0, 90), i.e. in the bottom layer the material axis *a* coincides with the θ^1 axis of the shell coordinate system, whereas in the upper layer the material axes are rotated by 90 degrees (see Fig. 3).
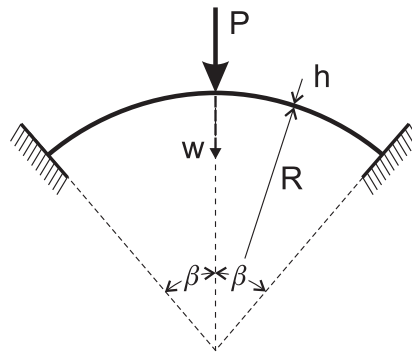
Fig. 7. Clamped shallow laminated arch

The obtained results are presented in Fig. 8 as the equilibrium paths in the space of the

non-dimensional load parameter, $\overline{P} = 10PR^2\beta/\pi^2EI$, and the central vertical deflection w.
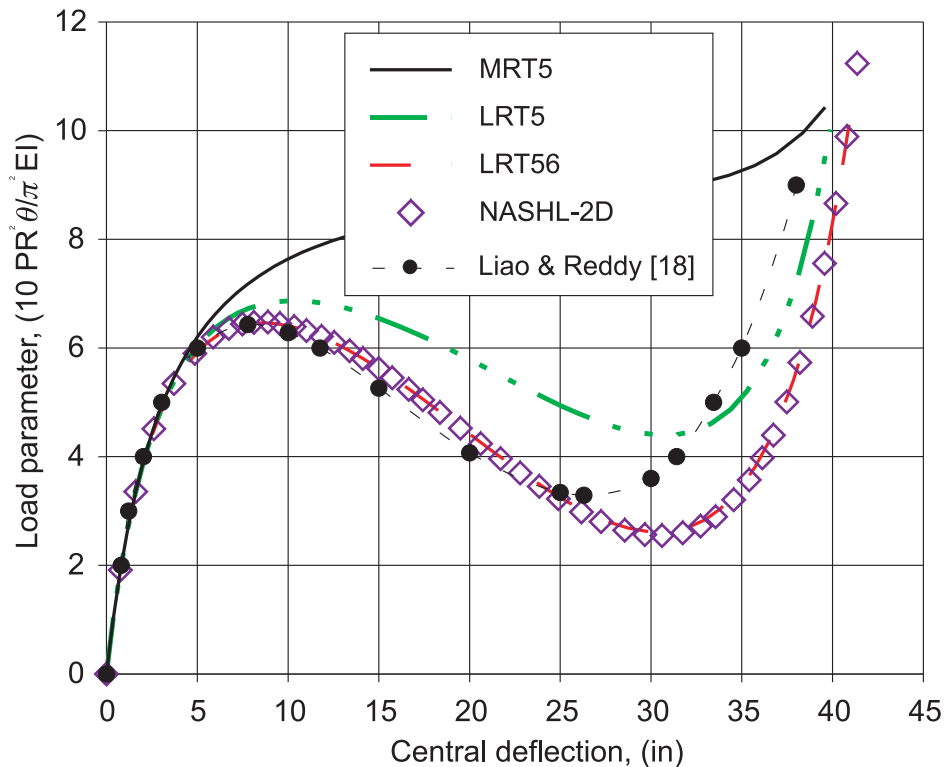
Fig. 8. Central vertical deflection for the clamped laminated arch

Looking at the evident differences in the responses obtained with the MRT5, LRT5 and the

LRT56 models one can conclude that the considered example deals with finite rotations. The

range of moderate rotations ends before the load parameter reaches the value 6 and,

consequently, the MRT5 solution does not predict the snap-through instability, which is

evident in both the large rotation formulations, LRT5 and LRT56. However, the lack of the

proper treatment of the rotations in the LRT5 approach is manifested by the overestimation of the maximum load level, and total disagreement with LRT56 in the post-buckling path. The maximum load level predicted by the LRT56 model agrees quite well with the reference solution [18] but the further part of their post-buckling path differs from the LRT56 response. To allow for the final verification of the obtained results additional computations have been performed for the analysed arch with the layered beam degenerated element with finite rotations (modified program NASH2D [58]) and a very good agreement has been obtained in the entire post-buckling range with the LRT5/6 solution.

3. 3. Asymmetric cross-ply simply supported plate strip

We consider a simply supported asymmetric laminate (0/90) as shown in Fig. 9 assuming the following data: $a = 9.0$ in, $b = 1.5$ in, $h = 0.04$ in, $E_1 = 2.0 \times 10^7$ lb/in^2, $\nu_{12} = 0.30$, $E_2 = 1.4 \times 10^6$ lb/in^2, $G_{12} = G_{23} = G_{13} = 0.7 \times 10^6$ lb/in^2.
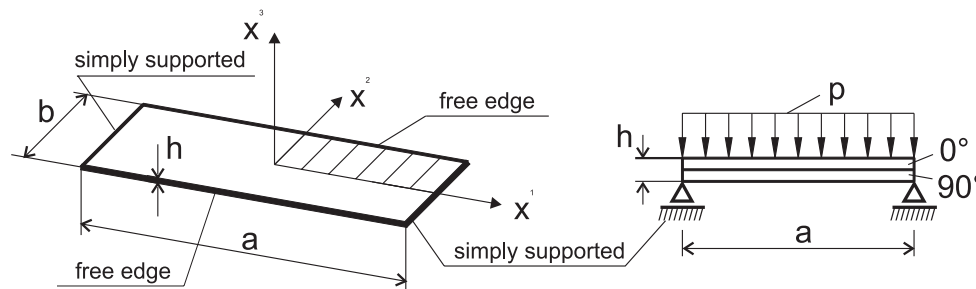
Fig. 9. Cylindrical bending of composite plate strip

This example was initially investigated by Sun and Chin [62], who presented large deflection cylindrical bending results of a pinned composite plate obtained with the von Kármán plate theory. Reddy [4], who analysed this problem with his Higher-Order Shear Deformation Theory, showed that really large deflections could be obtained for the simply

supported plate. Başar et al. [5] repeated this analysis using the Third-Order Shear Deformation Theory and fully non-linear formulation for finite rotations.

Due to the dual symmetry of the analysed structure, a quarter of the plate is modelled with nine 8-URI elements. The results obtained with the LRT56 approach are shown in Fig. 10.
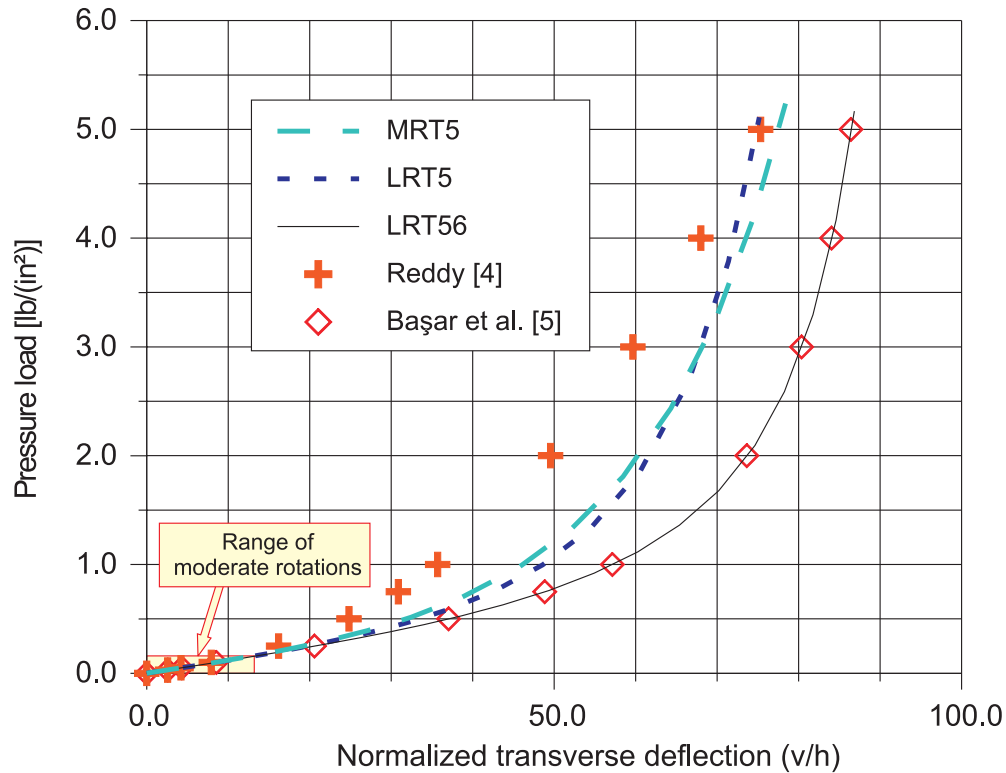

Fig. 10. Normalized central deflection of the plate strip under pressure load

Our LRT56 results agree very well with those of Başar et al. [5] what allows for the conclusion that in this example the refined representation of the transverse shear strains does not improve the accuracy of the solution. Both solutions are quite different from the results of Reddy [4], which is due to the fact that his model based on the von Kármán-type plate theory is not capable of dealing with large rotations. Reddy's solution [4] gives an acceptable prediction of the strip deflection only for the range $w/h < 10$, whereas our MRT5 model is capable of dealing with bigger deflections ($w/h < 17$), which are a little beyond the range of moderate rotations marked in Fig. 10. It is interesting that using the full non-linear strain-

displacement relations but without the proper updating of the rotations (model LRT5) one cannot obtain better results than with MRT5.

3. 4. Clamped laminated cylindrical panel under point load

We consider a deep cylindrical laminated $(0/90/0/90)_s$ panel (Fig. 11) as analysed by Tsai et al. [25] with the following data: $R = 12$ in, $L = 5.5$ in, $\beta = 0.5$, $h = 4\cdot0.01$ in, $E_{11} = 20.46\cdot10^6$ psi, $E_{22} = 4.092\cdot10^6$ psi, $\nu_{12} = 0.313$, $G_{12} = G_{13} = 2.53704\cdot10^6$ psi, $G_{23} = 1.26852\cdot10^6$ psi.
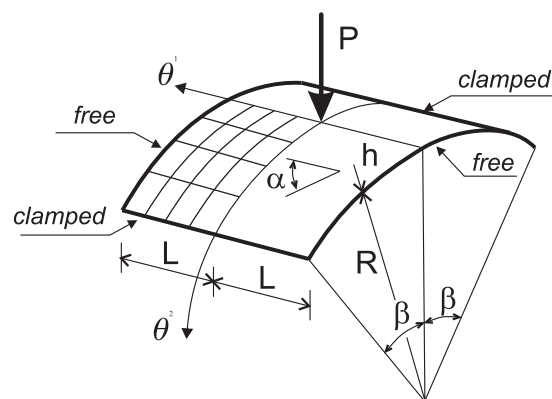
Fig. 11. Clamped laminated cylindrical panel under point load

The central deflection of the panel is shown in Fig. 12 versus the central load. One can notice that the buckling load level predicted with the present approach (LRT56) is in a quite good agreement with the solution given in [25]. Very similar results for the pre-buckling range have been also obtained with the LRT5 and MRT5 models. However, big differences appeared in the post-buckling range of the equilibrium path. The LRT56 solution is much closer to the reference solution [25] than the two other models but the difference is still significant. According to Tsai et al. [25], their model differs from the LRT56 in two aspects: 1) the transverse shear stress distribution is parabolic through the shell thickness; 2) linear strain-displacement relations are assumed for the transverse shear strains. To allow for more

adequate comparison of the results we have repeated the analysis with the modified model m-LRT56 created by dropping all non-linear terms in the transverse shear strains of LRT56.
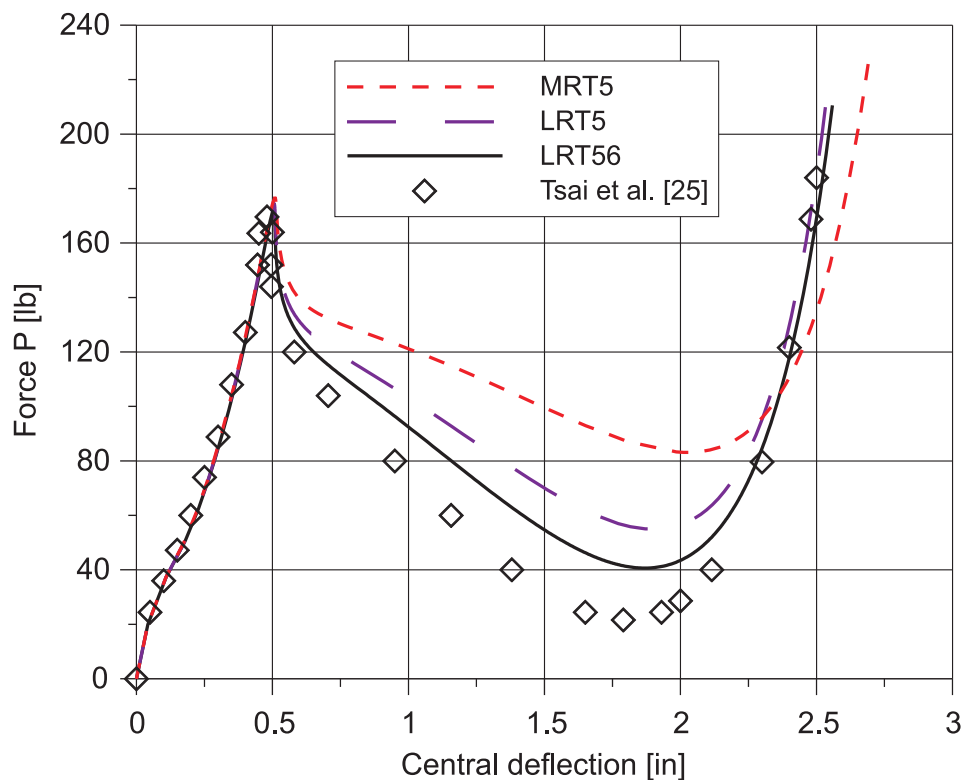

Fig. 12. Central deflection of the clamped laminated cylindrical panel under point load

Almost no difference between the results of m-LRT56 and LRT56 can be observed (see Fig. 13) what can support the opinion of Tsai et al. [25] that non-linear terms in the transverse shear strains are insignificant in the considered example. However, the m-LRT56 solution still is different from that given in [25]. In the second attempt the m-LRT5 model based on the LRT5 approach (i.e. dropping all non-linear terms in the transverse shear strains of LRT5) has been applied and this time the obtained results were almost identical with those of Tsai et al. [25]. The conclusions are the following:

a) similarly as in the LRT5 model, the formulation applied in [25] does not perform a proper updating of rotations;

b) the proper updating of the rotational degrees of freedom for thin composite shells can

be more essential for the accuracy of the solution than the refined representation of the

transverse shear strains.
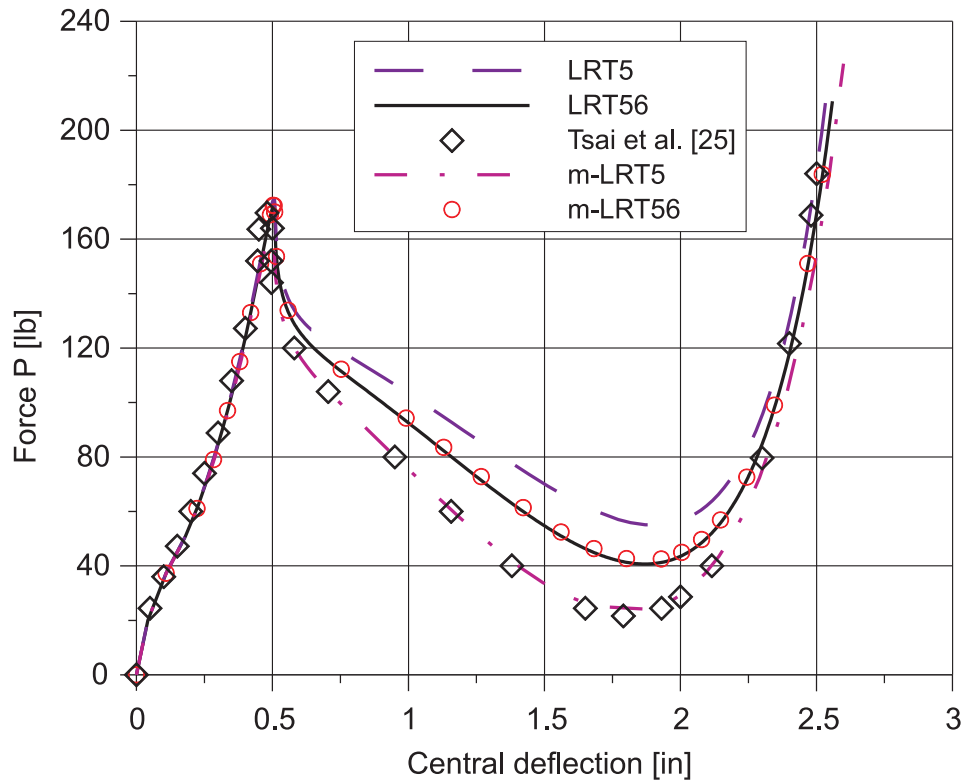
Fig. 13. Additional comparative study for the clamped cylindrical panel

An additional support for the above conclusions can be found in Table 2 where the

snap-through loads calculated for the clamped cylindrical panel with different models are

recorded.

One can observe a gradual decrease of the snap-through load with the increase of the accuracy

of the applied model - from 44.13 lb for MRT5, through 43.64 lb (LRT5), to 43.06 lb for

LRT56. The limit load given by Tsai et al. [25] is even lower - its level is equal to 42.4 lb[§]

what is very close to the value of 42 lb obtained in the m-LRT5 model where all nonlinear

terms were omitted for the transverse shear strains. However, it is worth to notice that the difference between the snap-through load estimated with the models m-LRT56 and LRT5 is insignificant.

Table 2.
Comparison of limit load for the clamped cylindrical panel

Model	snap-through load [lb]
MRT5	44.13
LRT5	43.64
LRT56	43.06
Tsai et al. [25]	42.4
m-LRT5	42.00
m-LRT56	43.13

3. 5. Stretching of an open cylinder

This example serves in the literature as one of the most demanding tests for the finite rotation analysis of isotropic shells (see e.g. [29], [63], [64] and [65]). Recently also a composite variant of this example has been proposed by Masud et al. [41]. The short cylinder (see Fig. 14) is loaded by two opposite stretching forces in its middle section; the ends of the cylinder are free. The geometry of the shell is characterized by the following data: R = 4.953 in, L =5.175 in, $\beta = 0.5$, h = 0.094 in. Due to the symmetry of the problem, only one octant of the cylinder is modelled with a regular mesh of 8x10 8-URI shell elements.

The results obtained for the isotropic variant (E = 10500 ksi and $v = 0.3125$) are presented in Fig.15 together with the reference solutions of Sansour & Bednarczyk [63], Chroscielewski [64] and Masud et al. [41]. The LRT56 solution is in a quite good agreement with the results of [63] and [64], while the solution given in [41] remains noticeably different.

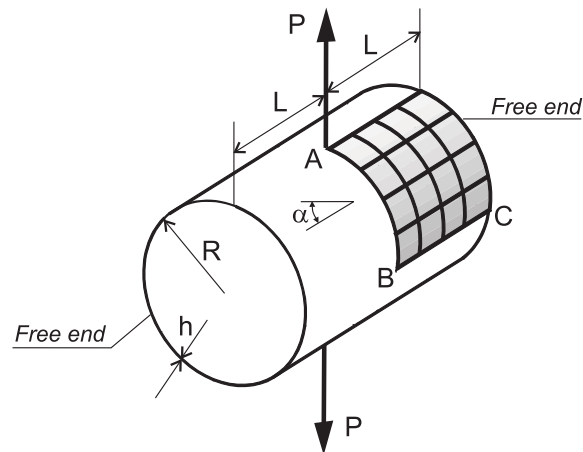§ This value was measured at the graph in [25].
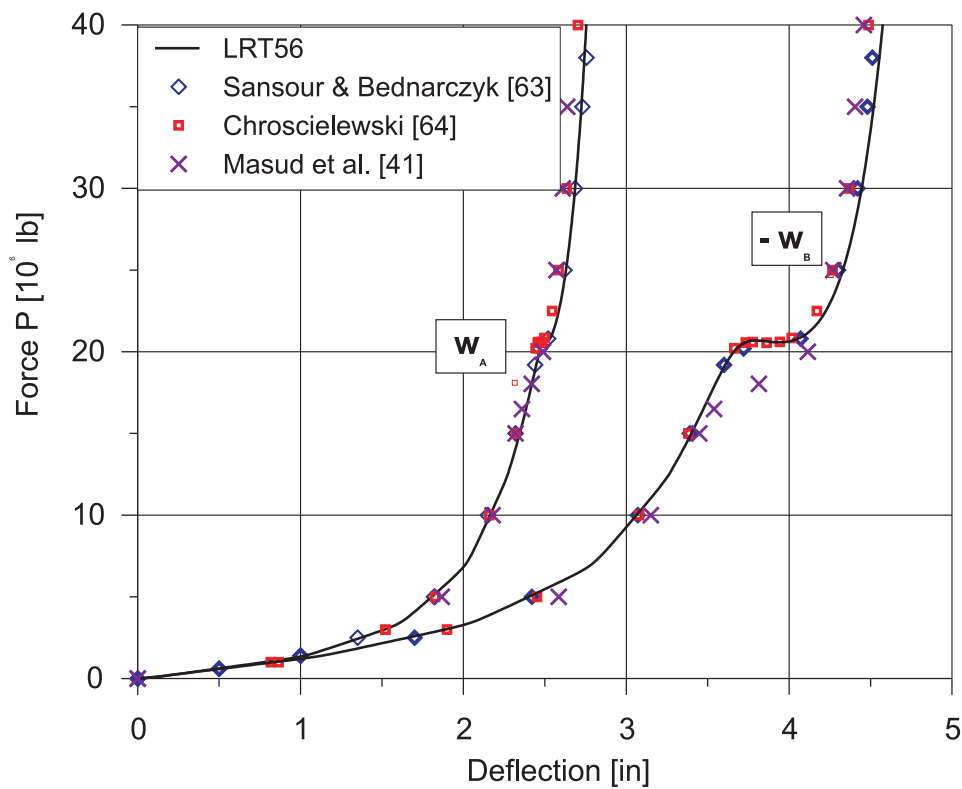
Fig. 14. Stretching of a short cylinder

Fig. 15. Radial deflections at points A and B for the isotropic cylinder

The next computations for the stretching of the free end cylinder are performed following

Masud et al. [41] for the laminated shell (0/90) with the following material properties

$E_{11} = 30500$ ksi, $E_{22} = 10500$ ksi, $G_{12} = G_{13} = G_{23} = 4000$ ksi and $\nu_{12} = 0.3125$.** The geometry

of the shell remains the same as given in Fig. 14. The radial displacement of the loaded point

A calculated with the LRT56 approach are compared in Fig. 16 with the reference solution

[41] using different density of the mesh.
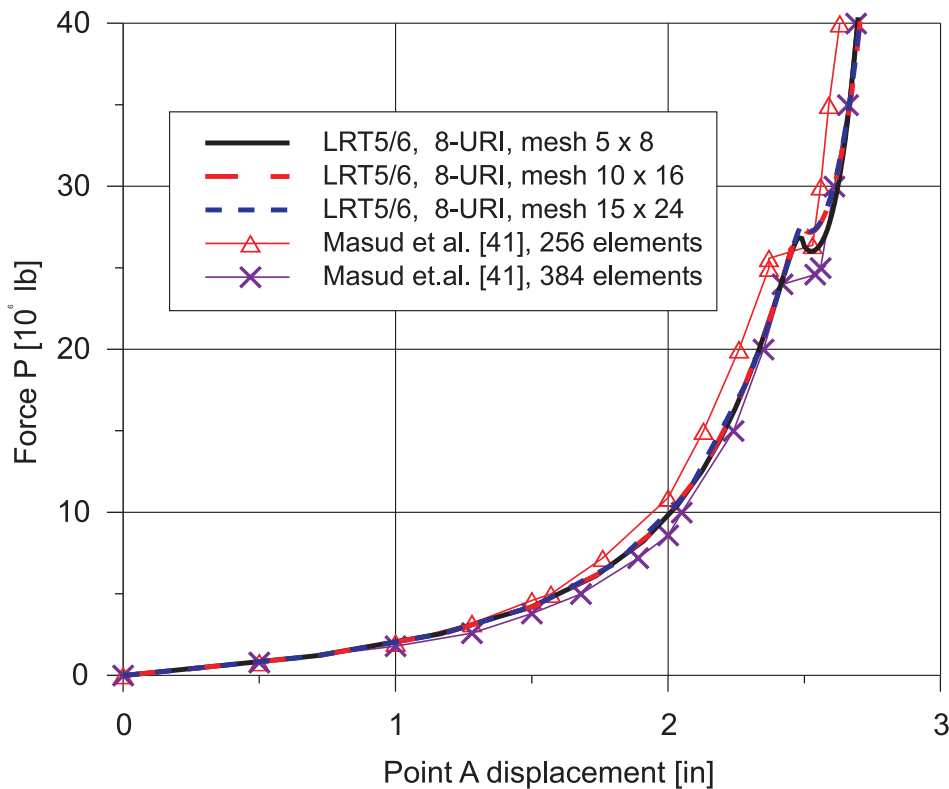
Fig. 16. Radial deflections at the point A for the composite cylinder

One can notice that differences between the reference solutions for 256 and 384 element

appear at a quite low load level, whereas the differences between 5x8 and 10x16 meshes of

the LRT56 model are visible only in the vicinity of the snap-through region. Increasing the

density of the mesh in the LRT56 approach from 10x16 to 15x24 elements resulted in almost

---

** Please notice, that the metric units used in [41] have been replaced here by USCS units to obtain more
reasonable data.

no change of the response. In contrary to [41], using the dense meshes in the LRT56 model a larger value of the snap-trough load is obtained than for the coarse mesh (5x8).

Interesting observations can be made when the LRT56 solution for the stretching of the composite cylinder is compared with the results of LRT5, MRT5 and MRT56[††] models (see Fig. 17). One can notice that the snap-through phenomenon is not manifested in the MRT5 or LRT5 results and both those models give stiffer response than the LRT56 approach or [41]. It is remarkable that the MRT56 model provides better estimation of the w_A displacement than the LRT5 approach. One can conclude that inclusion of additional terms in the LRT equations is not as much significant for the current example as the proper treatment of the rotational degrees of freedom.
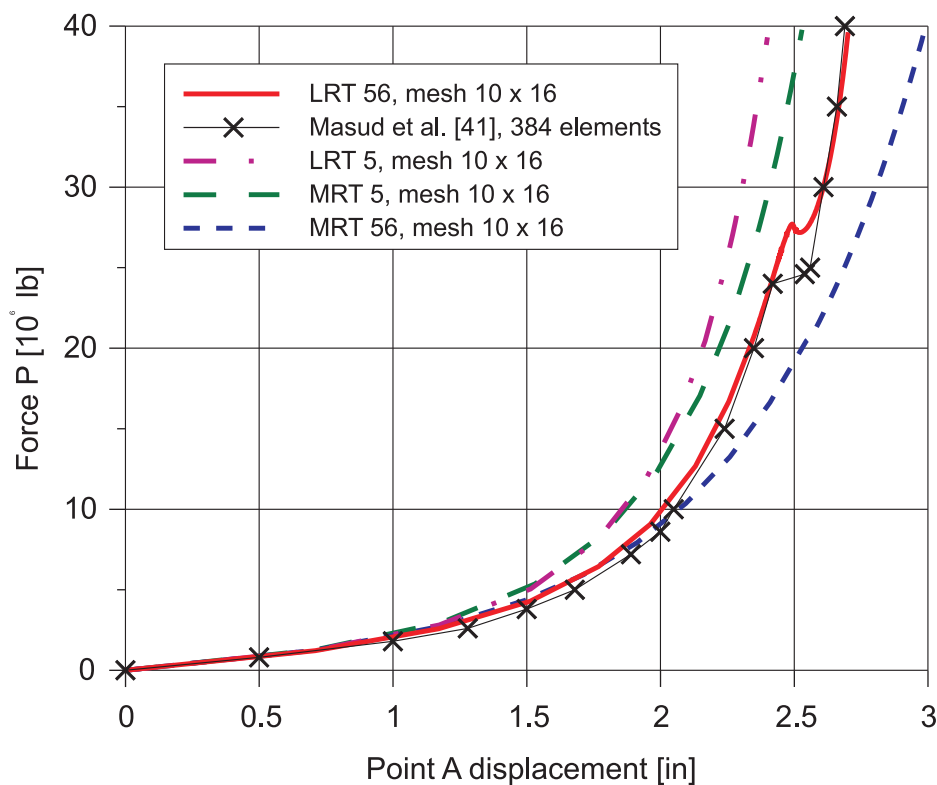

Fig. 17. Displacement at the point A for different models of the composite cylinder

[††] The MRT56 model consists of the MRT equations with the enhanced updating of rotations (analogous as used in the LRT56 approach).

The magnitude of the snap-through load for the stretching of the composite cylinder can be increased by 10% just by changing the order of the laminates from (0/90) to (90/0) as it is shown in Fig. 18.
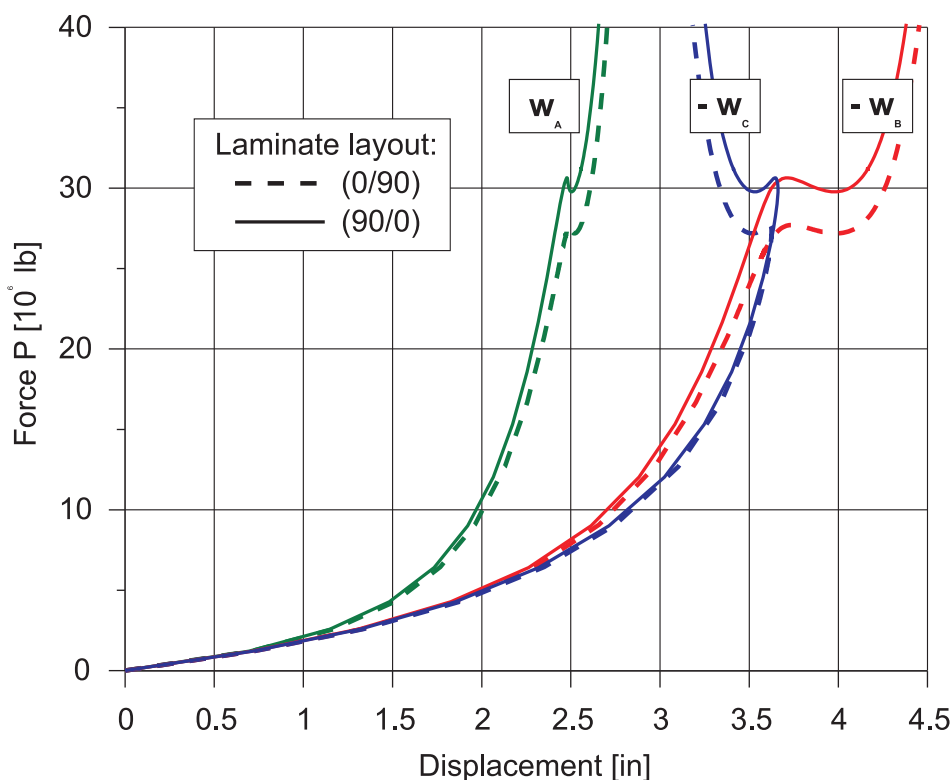

Fig. 18. Influence of the lamina sequence on the composite cylinder response in the stretching test

3. 6. Pinched hemispherical shell with 18° hole

In the last example we consider the probably most popular benchmark tests for finite rotation analysis of isotropic shells (see e.g. [30], [41], [49], [63] - [67]). The hemispherical shell with an 18 degree hole under two inward and two outward forces is presented in Fig. 19. The radius is R = 10 in and the thickness is h = 0.04 in. For the isotropic case the material properties are $E = 6825 \cdot 10^4$ psi and $v = 0.3$. Due to the double symmetry of the problem only one quarter of the shell is analysed with appropriate boundary conditions.
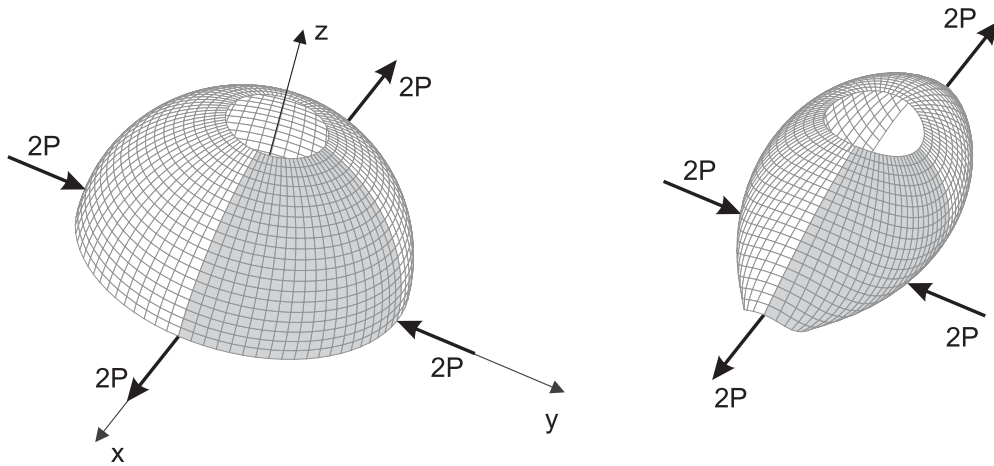
Fig. 19. Large deformation of a hemispherical shell with 18 degree hole

The numerical study has shown that a mesh of 12x12 elements 8-URI (regularly distributed in spherical coordinates) provides a convergent solution. The radial displacements of the shell computed within the LRT56 approach at the points subjected to the stretching and pinching forces, respectively, are presented in Fig. 20 together with selected reference solutions [30], [66] and [67]. An excellent agreement of results can be observed in Fig. 20 for the inward as well as for the outward deflection.
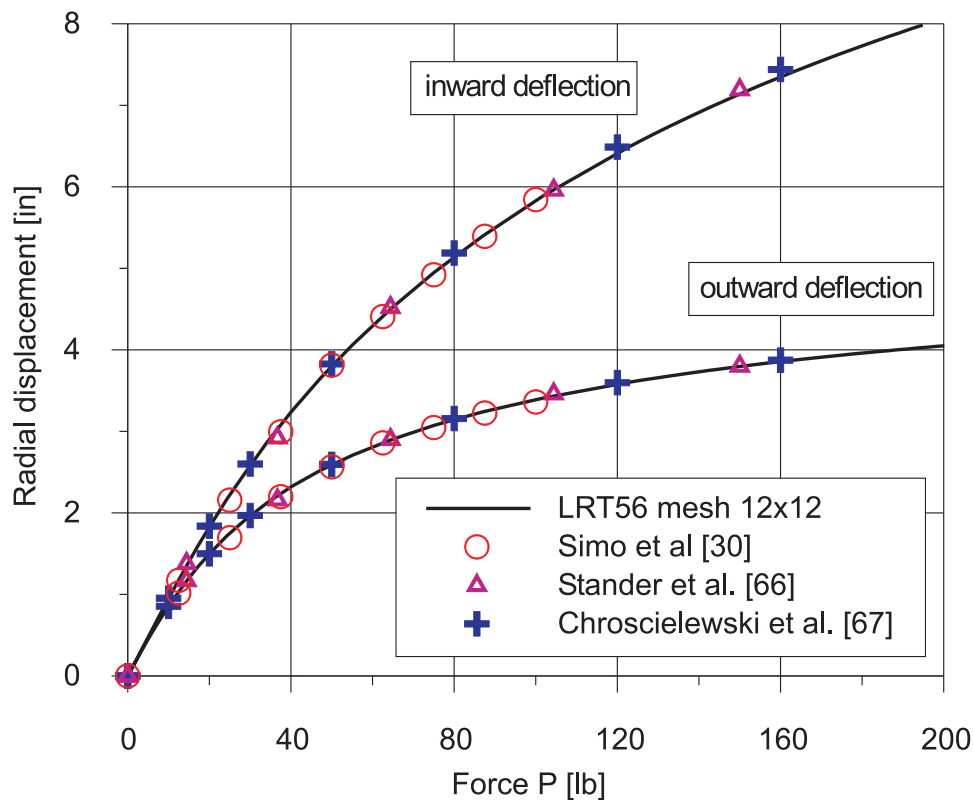

Fig. 20. Radial deflections of the isotropic hemispherical shell with 18 degree hole

Following the inspiration given in the previous example a composite variant of the hemispherical shell with 18 degree hole is considered next. To keep the analysed problem as realistic as possible the material data have been adopted from the paper by Tsai et al. [25] (compare Example 3.2): $E_{11} = 20.46 \cdot 10^6$ psi, $E_{22} = 4.092 \cdot 10^6$ psi, $G_{12} = G_{13} = 2.53704 \cdot 10^6$ psi, $G_{23} = 1.26852 \cdot 10^6$ psi and $\nu_{12} = 0.313$. To obtain a similar range of deflections as for the isotropic case the shell thickness has been increased to $h = 0.08$ in. Keeping in mind the hemispherical geometry of the analysed shell it was assumed that the fibre reinforcement (material axis 1 of the composite) is running in the circumferential direction (parallel to the equator). One should remember that the generating lines (meridians) do not keep the interval (distance) – in the considered example the length of the bottom edge of the shell is 3.24 times the length of the upper edge. The results of the LRT56 computations performed for the composite hemisphere are presented in Figures 21 and 22 together with the solutions computed with models RVK5, MRT5, LRT5 and m-LRT5. Since no reference solutions for the analysed problem are available in literature, the comparative calculations have been carried out in the MSC/NASTRAN computer code using QUAD4 elements in co-rotational formulation [68].

The graphs of the outward and inward radial deflections of the panel are shown in Fig. 21 in and in Fig. 22, respectively. The inward deflection is almost twice as big as the outward displacement, and differences among curves obtained for RVK5, MRT5, LRT5 and LRT56 models are much more significant in the second graph. However, the responses for the inward deflection obtained with MRT5 and LRT5 approaches are surprisingly similar. A very good agreement between the LRT56 model and the MSC/NASTRAN solution can be observed in both figures (Fig. 21 and Fig.22) and also in Table 3 presenting the values of the radial deflection for the load level P=160 lb.
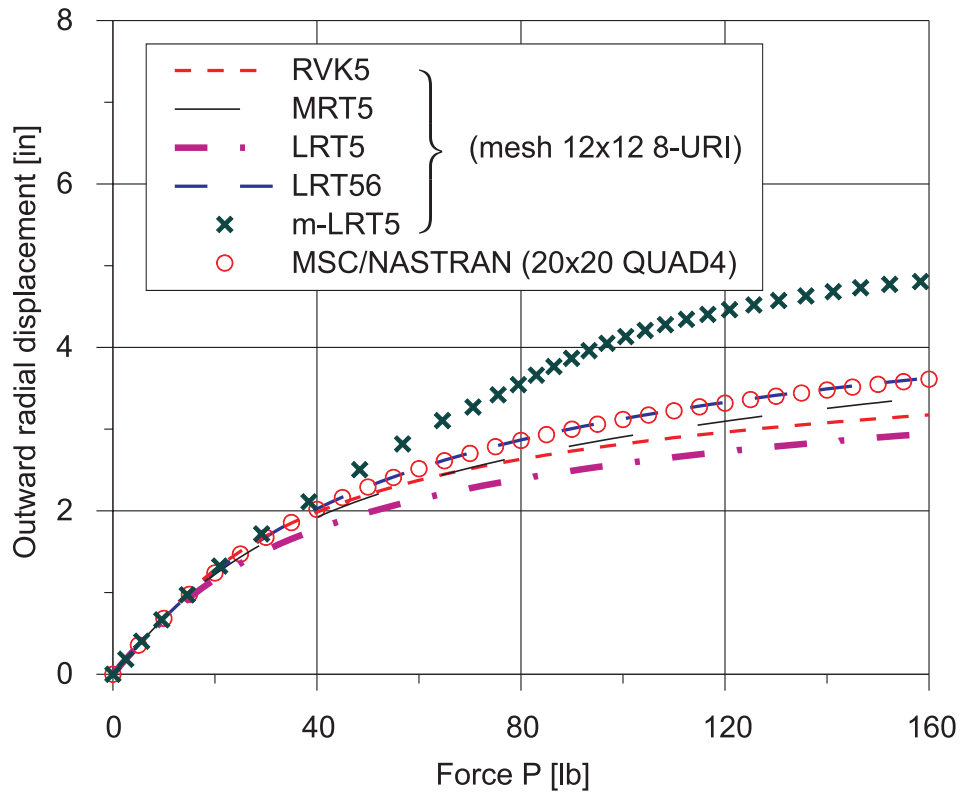
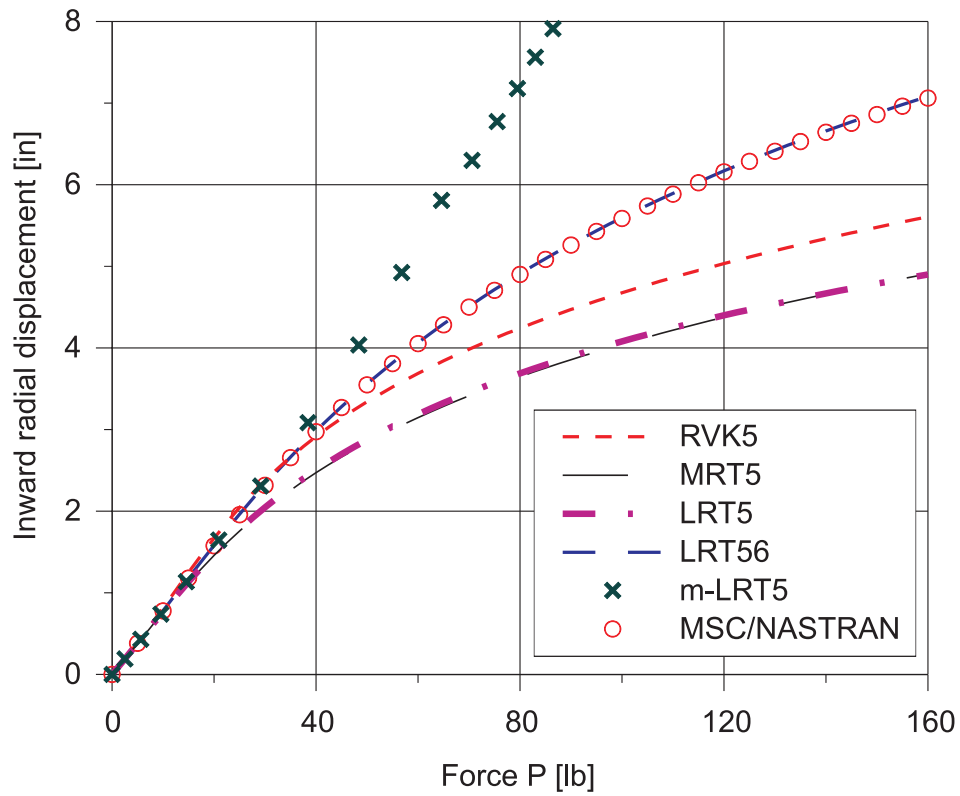Fig. 21. Outward radial deflection of the composite hemispherical shell

Fig. 22. Inward radial deflection of the composite hemispherical shell

Table 3.
Radial deflections of the composite hemispherical shell under P=160 lb

Model	Outward deflection [in]	Inward deflection [in]
RVK5	3.389	5.608
MRT5	3.627	4.908
LRT5	2.946	4.901
LRT56	3.627	7.082
MSC/NASTRAN	3.611	7.061
m-LRT5	4.813	11.798[*)]

[*)] this deflection is greater than the radius because one quarter of the shell has been used in the analysis

The influence of the circular fibre reinforcement on the response of the composite hemispherical shell is investigated in the following parametric study. It was assumed that all material parameters take the same values as before, except of $E_{11} = n \cdot E_{22}$, where n is the orthotropy ratio assuming values from the range (5 - 30). Such an assumption corresponds to increasing circular fibre reinforcement. The graph of the inward deflection calculated with the LRT56 model for different values of the orthotropy ratio is presented in Fig. 23. A gradual increase of the shell stiffness can be observed for increasing orthotropy ratio.
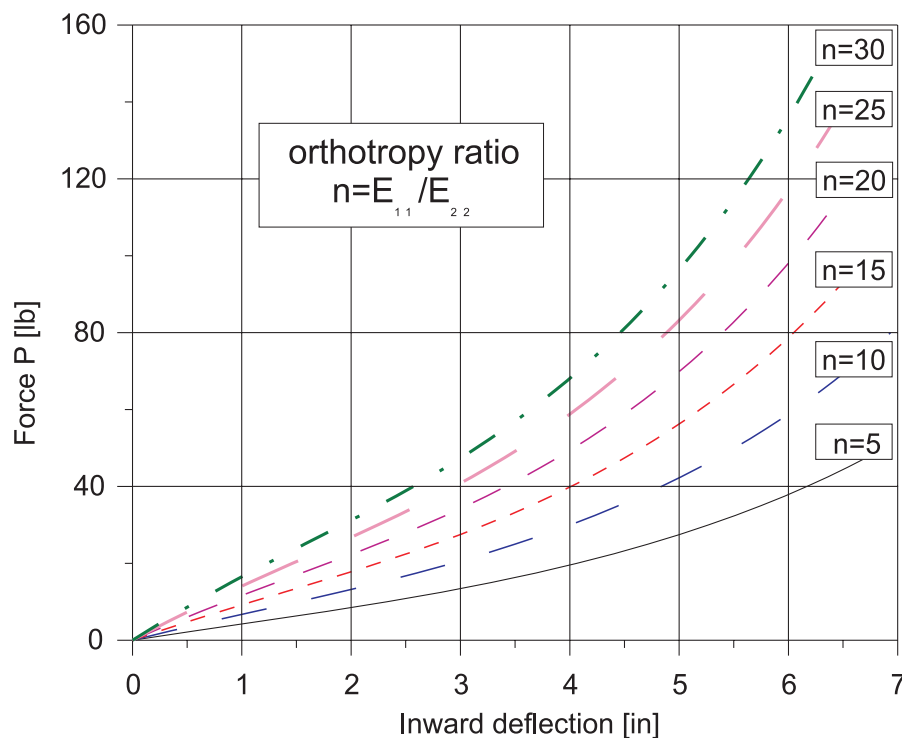

Fig. 23. Inward deflection of the hemispherical shell for different orthotropy ratio

A similar observation can be made in Fig. 24 where the values of the inward and outward deflections of the hemispherical shell are presented as a function of the orthotropy ratio, n, for the constant load level P = 60 lb.
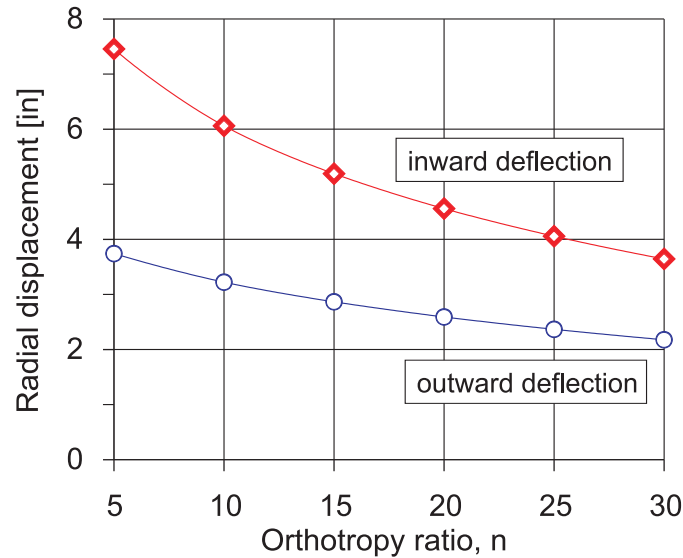

Fig. 24. Deflections for P = 60 lb as function of the orthotropy ratio

4. Conclusions

In this paper, an enhanced, accurate FE formulation of composite laminated shells undergoing large rotations based on the use of Euler angles is derived in the framework of the FOSD hypothesis. The main emphasis is put (a) on the exact treatment of large rotations in an incremental total Lagrangian formulation, (b) on the relevance of five- and six-parameter variants, respectively, of the FOSD hypothesis for large rotation plate and shell problems, (c) on the consequences of using approximate strain-displacement relations or an approximate approach to large rotations only.

Applying the six-parameter FOSD hypothesis and the concept of Euler angles to express the changes of the inextensible shell director, a numerical formulation based on the increments of five parameters only is developed. Using the obtained exact relations it can be shown that the five-parameter FOSD hypothesis, i.e. the assumption of constant through-thickness

distribution of the transverse normal displacements, is acceptable only for small and moderate rotation problems, while large rotation problems require a six-parameter approach admitting at least a linear through-thickness distribution of the transverse normal displacement even for inextensibility of the director. This leads to the conclusion that for large rotation shell analysis finite element methods based on five-parameter theories, which can be found even in recent literature, cannot be accepted. In fact, the theoretically observed shortcomings of five-parameter large rotation shell theories mentioned above become also evident in comparative finite element analysis, where often not only quantitative differences can be observed, but even a qualitatively different structural response is predicted.

Additionally, the comparative non-linear finite element analysis of various sample problems of non-linear, large rotation response of composite laminated plate and shell structures, including symmetric and asymmetric snap-through and snap-back problems, is extended to large rotation theories proposed in literature that use approximate strain-displacement relations or an approximate approach to large rotations only. From the obtained results, it can be concluded that the proper updating procedure of the rotations is of utmost importance as soon as the range of moderate rotations is exceeded. Additionally, approaches that use approximate strain-displacement relations by neglecting all non-linear terms in the transverse shear strain-displacement relations cannot be confirmed.

Finally, the authors take the liberty to point out again that the scope of the paper is limited to small strain static problems of elastic laminated shells of a perfect geometry. However, the sequel paper is under preparations which will deal with the buckling of laminated panels under axial compression including geometrical imperfections and thermal effects.

References

1   L. Librescu, *Elastostatics and Kinetics of Anisotropic and Heterogeneous Shell-Type Structures*, Noordhoff, Leyden (1975).

2   L. Librescu, Refined geometrically non-linear theories of anisotropic laminated shells, *Quarterly of Applied Mathematics* **45**, 1-22 (1987).

3   L. Librescu and R. Schmidt, Refined theories of elastic anisotropic shells accounting for small strains and moderate rotations, *Int. J. Non-Linear Mechanics* **23**, 217-229 (1988).

4   J. N. Reddy, A general non-linear third-order theory of plates with moderate thickness, *Int. J. Non-Linear Mechanics* **25**, 677-686 (1990).

5   Y. Başar, Y. Ding and R. Schultz, Refined shear-deformation models for composite laminates with finite rotations, *Int. J. Solids Structures* **30**, 2611-2638 (1993).

6   L. M. Habip, *Theory of Plates and Shells in the Reference State*, PhD Thesis, University of Florida (1964)

7   L. M. Habip, Theory of elastic shells in the reference state, *Ing.-Archiv.* **34**, 228-237 (1965).

8   L. M. Habip and I. K. Ebcioglu, On the equations of motion of shells in the reference state, *Ing.-Archiv.* **34**, 28-32 (1965).

9   R. Schmidt and J. N. Reddy, A refined small strain and moderate rotation theory of elastic anisotropic shells, *J. Applied Mech. Trans. ASME* **55**, 611-617 (1988).

10   G. A. Wempner, *Mechanics of Solids with Applications to Thin Bodies*, McGraw-Hill, New York (1973).

11   K. Z. Galimov, *Foundations of the Non-linear Theory of Shells* (in Russian), Kazan' University Press, Kazan' (1975).

12   K. Z. Galimov, *Theory of Shells with Transverse Shear Deformation Effect* (in Russian), Kazan' University Press, Kazan' (1977).

13   L. Librescu and R. Schmidt, Substantiation of a shear-deformable theory of anisotropic composite laminated shells accounting for the interlaminae continuity conditions, *Int. J. Engng. Sci.* **29**, 669-683 (1991).

14   R. Schmidt and L. Librescu, Further results concerning the refined theory of anisotropic laminated composite plates, *Int. J. Engineering Mathematics* **28**, 407-425, (1994).

15   L.A. Schmit Jr. and G.R. Monforton, Finite deflection Discrete Element Analysis of sandwich plates and cylindrical shells with laminated faces, *AIAA Journal* **8**, 1454-1461 (1970).

16   T. Y. Chang and K. Sawamiphakdi, Large deformation analysis of laminated shells by finite element method, *Computers & Structures* **13**, 331-340 (1981).

17   Jun, S. M., Hong, C. S., Buckling behavior of laminated composite cylindrical panels under axial compression, *Computers & Structures* **29**, 479-490 (1988).

18   C.-L. Liao and J. N. Reddy, *An Incremental Total Lagrangian Formulation for General Shell-Type Structures,* Virginia Polytechnic Institute, Rep. CCMS-87-16, (1987).

19   G. Laschet and J.-P. Jeusette, Postbuckling finite element analysis of composite panels, *Composite Structures* **14**, 35-48 (1990).

20   S. Saigal, R. K. Kapania and T. Y. Yang, Geometrically nonlinear finite element analysis of imperfect laminated shells, *J. Composite Materials* **20**, 197-214 (1986).

21   A. J. M. Ferreira and J. T. Barbosa, Buckling behaviour of composite shells, *Composite Structures* **50**, 93-98 (2000).

22   A. F. Palmerio, J. N. Reddy and R. Schmidt, On a moderate rotation theory of elastic anisotropic shells - Part 2: FE analysis, *Int. J. Non-Linear Mechanics* **25**, 701-714 (1990).

23   I. Kreja, R. Schmidt and J. N. Reddy, Finite elements based on the first-order shear deformation moderate rotation shell theory with applications to the analysis of composite structures, *Int. J. Non-Linear Mechanics* **32**, 1123 -1142 (1997).

24   S. T. Dennis and A. N. Palazotto, Large displacement and rotational formulation for laminated shells including parabolic transverse shear, *Int. J. Non-Linear Mechanics* **25,** 67-85 (1990).

25   C. T. Tsai, A. N. Palazotto and S. T. Dennis, Large-rotation snap-through buckling in laminated cylindrical panels, *Finite Elements in Analysis and Design* **9** (1991), 65-75.

26   V. Ferro, *Analyse géométriquement non linéaire des plaques en grandes rotations*, Ph.D. thesis, EUDIL, Univ. des Sciences et Tech de Lille, Villeneuve D'Ascq, France, 1998.

27   B. Bouhafs, K. Woznica and P. Klosowski, The large rotations theory of elasto-viscoplastic shells subjected to the dynamic and thermal loads, *Engineering Computations* **20**, 366-389. (2003).

28   P. Klosowski and K. Woznica, Numerical treatment of elasto viscoplastic shells in the range of moderate and large rotations, *Computational Mechanics* (2004) *(accepted for publication)*.

29   B. Brank, D. Peric and F. B. Damjanic, On implementation of a nonlinear four node shell finite element for thin multilayered elastic shells, *Computational Mechanics* **16**, 341-359 (1995).

30   J. C. Simo, D. D. Fox and M. S. Rifai, On a stress resultant geometrically exact shell model. Part III: Computational aspects of the nonlinear theory, *Comput. Methods Appl. Mech. Engrg.* **79**, 21-70 (1990).

31   E. Carrera and H. Parisch, An evaluation of geometrical nonlinear effects of thin and moderately thick multilayered composite shells, *Composite Structures* **40**, 11-24 (1998).

32   Y. Başar, M. Itskov and A. Eckstein, Composite laminates: nonlinear interlaminar stress analysis by multi-layer shell elements, *Comput. Methods Appl. Mech. Engrg.* **185**, 367-397 (2000).

33   B. Brank and E. Carrera, A family of shear-deformable shell finite elements for composite structures, *Computers and Structures* **76**, 287-297 (2000).

34   L.Vu-Quoc, H. Deng and X. G. Tan, Geometrically-exact sandwich shells: The static case, *Comput. Methods Appl. Mech. Engrg.* **189**, 167-203 (2000).

35   M. Balah and H. N. Al-Ghamedy, Finite element formulation of a third order laminated finite rotation shell element, *Computers & Structures* **80**, 1975-1990 (2002).

36   S. Kinkel, F. Gruttmann and W. Wagner, A continuum based three-dimensional shell element for laminated structures, *Computers and Structures* **71**, 43-62 (1999).

37   G. M. Kulikov and S. V. Plotnikova, Non-linear strain-displacement equations exactly representing large rigid-body motions. Part I: Timoshenko-Mindlin shell theory, *Comput. Methods Appl. Mech. Engrg.* **192**, 851-875 (2003).

38   K. Y. Sze and S.-J. Zheng, A stabilized hybrid-stress solid element for geometrically nonlinear homogeneous and laminated shell analyses, *Comput. Methods Appl. Mech. Engrg.* **191**, 1945-1966 (2002).

39   K. D. Kim, Buckling behaviour of composite panels using the finite element method, *Composite Structures* **36**, 33-43 (1996).

40   K. Kim and G.Z. Voyiadjis, Non-linear finite element analysis of composite panels, *Composites, Part B* **30**, 365-381 (1999).

41   A. Masud, C. L. Tham and W. K. Liu, A stabilized 3-D co-rotational formulation for geometrically nonlinear analysis of multi-layered shells, *Computational Mechanics* **26**, 1-12 (2000).

42   K. D. Kim, G. R. Lomboy and S. C. Han, A co-rotational 8-node assumed strain shell element for postbuckling analysis of laminated composite plates and shells, *Computational Mechanics* **30**, 330-342 (2003).

43   P. F. Pai and A. N. Palazotto, Nonlinear displacement based finite element analysis of composite shells - A new total Lagrangian formulation, *Int. J. Solids Structures* **32**, 3047-3073 (1995).

44   M. R. Wisnom, The effect of fibre rotation in ± 45º tension tests on measured shear properties, *Composites* **26**, 25-32 (1995).

45   P. F. Pai and A. N. Palazotto, Large-deformation analysis of flexible beams, *Int. J. Solids Structures* **33**, 1335-1353 (1996).

46   J. M. Greer, Jr. and A. N. Palazotto, Application of a total Lagrangian Corotational FE scheme to inflation of tires, *Int. J. Solids Structures* **34**, 3541-3570 (1997).

47   Y. Başar and O. Kintzel, Finite rotations and large strains in Finite Element shell analysis, *Comput Model Eng Sciences* **4**, 217-230 (2003).

48   G. A. Korn and T. M. Korn, *Mathematical Handbook for Scientists and Engineers*, Dover Publications, Inc. Minaola, New York (2000).

49   P. Betsch, A. Menzel and E. Stein, On the parametrization of finite rotations in computational mechanics, A classification of concepts with application to smooth shells, *Comput. Methods Appl. Mech. Engrg.* **155**, 273-305 (1998).

50   E. Ramm, and A. Matzenmiller, Large deformation shell analyses based on the degeneration concept, *Finite Element Methods for Plate and Shell Structures*, Vol.1: Element Technology, 365-393, eds. T.J.R. Hughes, E. Hinton, Pineridge Press Ltd., Swansea (1986).

51   K.-J. Bathe, *Finite Element Procedures*, Prentice Hall Inc., New Jersey (1996).

52   M. Kleiber, *Incremental Finite Element Modeling in Non-Linear Solid Mechanics*, J. Wiley & Sons, New York (1989).

53   F. Frey and S. Cescotto, Some new aspects of the incremental Total Lagrangian description in nonlinear analysis, *Proc. Int. Conf. on Finite Elements in Nonlinear Solid and Structural Mechanics*, Geilo, Norway, 1977, Vol.1, 323-343, ed. Bergan, P. G. et al., Tapir Press, Norwegian Institute of Technology, Trondheim (1977).

54   K. S. Surana, Geometrically nonlinear formulation for the axisymmetric shell elements, *Int. J. Num. Meth. Engng* **18**, 477-502 (1982).

55   K. S. Surana, A generalized geometrically nonlinear formulation with large rotations for finite elements with rotational degrees of freedoms, *Computers & Structures* **24**, 47-55 (1986).

56   E. Ramm, Strategies for tracing the nonlinear response near limit points, *Proc. Europe-US Workshop on Nonlinear finite element analysis in structural mechanics*, Bochum 1980, 63-89, eds. W. Wunderlich et al., Springer-Verlag (1981).

57   D. A. DaDeppo and R. Schmidt, Instability of clamped-hinged circular arches subjected to a point load, *J. Applied Mech. Trans. ASME* **42**, 894-896 (1975).

58   I. Kreja and Z. Cywinski, Degenerated isoparametric finite elements in nonlinear analysis of 2D-problems, *Computers & Structures* **41**, 1029-1040 (1991).

59   M. Li, The finite deformation theory for beam, plate and shell. Part I. The two-dimensional beam theory, *Comput. Methods Appl. Mech. Engrg*. **146**, 53-63 (1997).

60   R. K. Kapania and J. Li, A formulation and implementation of geometrically exact curved beam elements incorporating finite strains and finite rotations, *Computational Mechanics* **30**, 444-459 (2003).

61   J. C. Simo, P. Wriggers, K. H. Schweizerhof and R. L. Taylor, Finite deformation postbuckling analysis involving inelasticity and contact constraints, *Int. J. Num. Meth. Engng* **23**, 775-800 (1986).

62   C. T. Sun, H. Chin, Analysis of Asymmetric Composite Laminates, *AIAA Journal* **26**, 714-718 (1988).

63   C. Sansour and H. Bednarczyk, The Cosserat surface as a shell model, theory and finite-element formulation, *Comput. Methods Appl. Mech. Engrg*. **120**, 1-32 (1995).

64   J. Chroscielewski, *Family of C^0 finite elements in six-parameter non-linear theory of shells* (in Polish), Zeszyty Naukowe Politechniki Gdanskiej (Proceedings of GUT), **540**, (1996)

65   R. A. Fontes Valente et al., On the use of an enhanced transverse shear strain shell element for problems involving large rotations, *Computational Mechanics* **30**, 286-296 (2003).

66   N. Stander, A. Matzenmiller and E. Ramm, An assessment of assumed strain methods in finite rotation shell analysis, *Eng. Comput*., **6**, 58-66 (1989).

67   J. Chroscielewski, J. Makowski and H. Stumpf, Finite element analysis of smooth, folded and multi-shell structures, *Comput. Methods Appl. Mech. Engrg*. **141**, 1-46 (1997).

68   *MSC/NASTRAN for Windows installation and application manual,* MacNeal-Schwendler Corporation (1995).